RHODOPSIN 7: An ancient non-retinal photoreceptor for contrast vision, darkness detection, and circadian regulation

Valentina Kirsch[1], Nils Reinhard[1], Heiko Hartlieb[1], Annika Mohr[1], Dirk Rieger[1], Peter Soba[2], Charlotte Helfrich-Förster[1], Pingkalai R. Senthilan[1]

[1] Neurobiology and Genetics, Theodor-Boveri Institute, Biocenter, Julius-Maximilians-University Würzburg, 97074, Würzburg, Germany

[2] Institute of Physiology and Pathophysiology, Friedrich-Alexander-Universität Erlangen-Nürnberg, 91054, Erlangen, Germany

1 Abstract

Animals rely on light not only for vision but also to adapt behavior to their environment. In *Drosophila*, most rhodopsins mediate retinal image formation, but RHODOPSIN 7 (RH7) is widely expressed in the brain and optic lobe, acting as a non-retinal light sensor reminiscent of mammalian melanopsin. We combined expression mapping, behavioral assays, and phylogenetic comparisons to investigate its function. RH7 detects light-on and light-off transitions, modulates contrast, motion, and brightness perception, and contributes to circadian clock synchronization. Flies lacking RH7 are less active during the dark phase, while strains with constitutively active protein show increased activity. Phylogenetic analyses suggest that RH7 is an ancient rhodopsin present across panarthropods, representing an intermediate between G protein-coupled receptors and specialized rhodopsins, highlighting a key step in the evolution of non-visual light perception. These findings show that RH7 functions as a melanopsin-like sensor, shaping behavior and illuminating the origins of light detection.

2 Introduction

The ability to detect and respond to light is fundamental for many organisms. Vision relies on specialized photoreceptor cells that convert light into neural signals through a process called phototransduction. This allows the brain to interpret visual information and guide behavior. The rhodopsin chromoproteins, composed of the seven-helix membrane apoprotein opsin and the chromophore retinal, play a central role in this process. When a photon is absorbed, the chromophore undergoes a conformational change, transforming from 11-cis-3-hydroxyretinal to all-trans-3-hydroxyretinal. Then, structural changes occur in the protein, initiating signal transduction. As G protein-coupled receptors (GPCRs), rhodopsins first activate a trimeric G

protein, which then initiates a cascade of downstream signaling events in phototransduction (Xiong and Bellen, 2013).

While the primary function of rhodopsins is image formation, some are also known to participate in non-image-forming functions. Based on their specific roles, rhodopsins are classified as visual or non-visual (Kingston and Cronin, 2016; Leung and Montell, 2017; Terakita, 2005). Several studies have highlighted the diverse functions of rhodopsins, including their involvement in thermosensation (Shen et al., 2011), hearing (Senthilan et al., 2012), proprioception (Zanini et al., 2018), and taste (Leung et al., 2020).

Opsins are classified into different groups, including c-opsins (ciliary) and r-opsins (rhabdomeric). While c-opsins trigger a $G_{\alpha}t$ (G_{alpha} transducin)-mediated signaling pathway leading to Na^+ channel closure and consequent hyperpolarization, r-opsins trigger a $G_{\alpha}q$-mediated depolarizing signaling cascade. In humans, c-opsins in rods and cones are essential for visual perception, while melanopsin (OPN4), an r-opsin expressed in intrinsically photosensitive retinal ganglion cells (ipRGCs), is involved in the synchronization of circadian rhythms and enhances contrast sensitivity (Sonoda et al., 2018). *Drosophila melanogaster* (*Dmel*) has seven rhodopsins (RH1-RH7), all belonging to the r-opsin group. RH1 (RHODOPSIN 1), the primary rhodopsin, is encoded by the *ninaE* (*neither inactivation nor afterpotential E*) gene and is expressed in the outer receptor cells R1-R6 of the retina in the compound eyes of flies. These cells project to the monopolar cells in the lamina, where the signals are processed and transmitted to the medulla. The inner receptor cells R7 (expressing RH3 and RH4) and R8 (expressing RH5 and RH6) form synapses directly within the medulla. The medulla receives all signals, processes them further, and transmits them to the lobula and lobula plate. The R8 rhodopsins, RH5 and RH6, are also expressed in the larval eye, Bolwig's organ, and its adult remnant, the Hofbauer-Buchner (H-B) eyelet. RHODOPSIN 2 (RH2) is mainly expressed in the ocelli, while the expression of RHODOPSIN 7 (RH7) remains debated.

Phylogenetically*, Drosophila* rhodopsins cluster into three groups: The first group comprises RH3, RH4 and RH5; the second group consists of RH1, RH2 and RH6; and the last group is formed only by RH7. Homologs of RH7 occur broadly across arthropods, including hexapods, crustaceans, and chelicerates (Feuda et al., 2016; Senthilan and Helfrich-Förster, 2016). While the first six rhodopsins are well characterized, the function of RH7 remains unclear. RH7 shares typical rhodopsin features (seven transmembrane helices, chromophore-binding lysine, LRTPXN motif) but differs in having extended N- and C-terminal tails twice as long as in other rhodopsins (Figure 1A) (Senthilan and Helfrich-Förster, 2016). Moreover, RH7 and its homologs lack the highly conserved QAKKMNV motif in the third intracellular loop (ICL3), important for G protein interaction (Figure 1A, Supplementary Material S2A) (Senthilan and Helfrich-Förster, 2016). Unlike other rhodopsins, whose non-palindromic RCSI (Rhodopsin

Core Sequence I) motif lies ~100 bp upstream of their transcription start sites, the RCSI of *Rh7* is fully palindromic (TAATCAGATTA) and located within its second intron, about 7 kb downstream of the transcription start site. Generally, the unique, non-palindromic RCSI sequences regulate cell-specific rhodopsin expression, while palindromic sequences correlate with broader gene expression (Datta and Rister, 2022; Rister et al., 2015; Senthilan and Helfrich-Förster, 2016). The unusual palindromic RCSI sequence, along with its positioning within the *Rh7* gene, may account for the distinct and broader expression of *Rh7*, which is consistent with TAPIN (tandem affinity purification of INTACT nuclei)-seq data. These data show that *Rh7* is absent in retinal photoreceptors but present in visual processing neurons in the lamina and medulla (Figure 1B) (Davis et al., 2020).

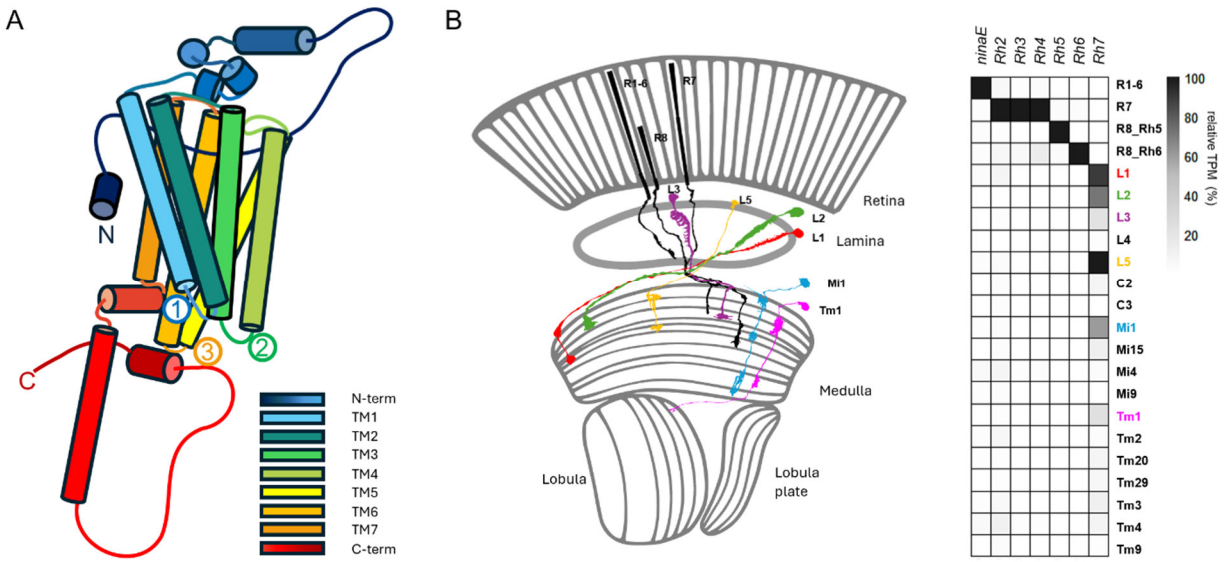

Figure 1 A) Schematic representation of the predicted 3D structure of RH7 (GH14208p) based on AlphaFold (Jumper et al., 2021). The structure is color-coded using a continuous spectral gradient ranging from blue (N-terminus) to red (C-terminus). The three intracellular loops are highlighted and labeled in numbered circles: (1) ICL1 with the LRTPXN motif, (2) ICL2 with the highly conserved DRY motif, and (3) ICL3, which lacks the typical QAKKMNV motif. The original illustration of AlpfaFold is shown in Supplementary Material S2A. B) Left: Schematic representation of the Drosophila melanogaster optical system. The presumed Rh7-expressing cells, according to Davis et al., (2020) are shown in addition to retinal receptor cells (black). Right: Heatmap of relative gene expression across Drosophila optic lobe cell types. TPM values were obtained by TAPIN sequencing (Davis et al., 2020) and normalized per gene (100 % = maximum TPM per gene). Color scale: white (0 %), light gray (~50 %), black (100 %). Genes are shown on the x-axis, and cell types on the y-axis.

Previous studies on the expression and function of RH7 have been contradictory (Grebler et al., 2017; Kistenpfennig et al., 2017; Leung et al., 2020; Leung and Montell, 2017; Ni et al., 2017; Senthilan et al., 2019). Two factors may explain these discrepancies. First, the genetic background of the tested flies, particularly the presence of the *white* and *yellow* mutations as markers, appears to influence the *Rh7* phenotype, possibly due to overlapping expression sites (Davis et al., 2020). Second, RH7 is relatively large but likely adopts a compact, self-contained structure (Figure 1A). Its highly phosphorylatable N and C termini may interact with other proteins and further obscure relevant epitopes, making antibody detection nearly impossible.

However, all previous studies, despite their differences, agree that *Rh7* is an atypical rhodopsin with non-visual functions, a hypothesis that is further supported by this study. We show that RH7 is distinct from other *Drosophila* rhodopsins. RH7 is expressed in non-retinal neurons and likely acts via a different signaling pathway, contributing to darkness detection and nocturnal activity. As an ancient rhodopsin, RH7 may support basic visual functions such as contrast processing and circadian synchronization, similar to melanopsins in mammals.

3 Material & Methods

3.1 Bioinformatics

We searched for r-opsin homologs in selected animals of the Protostomia using BLASTP from NCBI (blast.ncbi.nlm.nih.gov/Blast.cgi?PAGE=Proteins, accessed December 2023). Amino acid sequences of *Drosophila melanogaster* RH1-RH7 served as reference queries. Searches were performed against the non-redundant protein database (nr) using the default BLASTP settings (BLOSUM62 matrix, gap costs 11/1, conditional compositional score matrix adjustment). From the initial output, we curated a representative dataset of 53 species, prioritizing those with RH7 homologs. Protein hits were compiled in Excel and imported into Geneious Prime (2025.1.3) for downstream analysis. In total, more than 400 sequences were retrieved. Multiple sequence alignments were performed using global alignment with BLOSUM62 and gap costs of 11/1. A phylogenetic tree was generated using the neighbor-joining method with the Jukes-Cantor distance model. To minimize redundancy due to isoforms, gene duplications, or duplicate annotations, the dataset was manually curated across multiple iterations, resulting in a final set of 280 unique sequences. Protein names, sequences, and accession numbers are provided in Supplementary Material S1. To confirm phylogenetic assignments, reciprocal BLAST searches were performed against the *D. melanogaster* proteome, ensuring clade consistency and homology validation.

3.2 GsX assay

G protein coupling of GPCR constructs was examined using HEK293T or HEK293-ΔG7 cells (lacking GNAS, GNAL, GNAQ, GNA11, GNA12, GNA13, and GNAZ) obtained from A. Inoue at Tohoku University (Bowin et al., 2019). HEK293T cells were cultured in DMEM supplemented with 10% FBS (Pan Biotech, Germany), 100 U/mL penicillin and 100 mg/mL streptomycin at 37 °C in 5% CO_2. The GsX assay was modified from Ballister et al. (Ballister et al., 2018). White 96-well plates (Greiner Bio-One) were coated with 0.1 mg/mL poly-L-lysine (Sigma Aldrich, USA) at 37 °C for 1 h prior to cell seeding. Receptor plasmids, G-protein chimeras and Glo22F (Promega) were co-transfected using Lipofectamine 2000 (Thermo Fisher, USA) and incubated at 37 °C in 5% CO_2 for 24 hours. The medium was replaced with

130 L-15 medium (phenol red-free, 1% FBS) containing 2 mM beetle luciferin (in 10 mM HEPES,
131 pH 6.9) and 10 mM 9-cis-retinal or all-trans retinal and incubated for 1 hour at room
132 temperature in the dark. cAMP-dependent luminescence was measured using a Berthold
133 Mithras multimode plate reader (Berthold Tech., Germany). Cells were activated with a 1-
134 second light pulse (470 nm) using an LED light plate (Phlox Corp., France) or CoolLED pE-
135 4000 (CoolLED, UK). Two technical duplicates were performed, and data were normalized to
136 pre-activation baselines.

137 ### 3.3 Locomotor Activity

138 The locomotor activity of individual male flies was monitored at 1-minute intervals using the
139 *Drosophila* Activity Monitoring (DAM) system (Trikinetics, Inc., Waltham, MA), which detects
140 infrared (IR) beam interruptions. Male flies (3 to 7 days old) were individually placed in
141 recording glass tubes (~5 mm diameter) containing agar/sugar medium (2% agar; 4% sucrose)
142 filled to one-third capacity and sealed with an air-permeable plug. Activity was quantified by
143 counting the number of infrared (IR) beam crossings in the center of each tube. All recordings
144 were performed under constant conditions of 60% relative humidity and 25 °C, except for the
145 "hot day" experiments. For "hot day" experiments, the DAM monitors were placed inside a
146 programmable incubator (I-36NL; Percival Scientific, Inc., Perry, IA) to simulate temperature
147 cycles as described by Yoshii et al. (2009) and Bywalez et al. (2012). A "normal day" was
148 defined as 12 h light (30 μW/cm^2 corresponding to 100 lux) and 12 h darkness, while "short
149 days" consisted of 8 h light (30 μW/cm^2) and 16 h darkness. To assess light-off startle
150 responses, which are brief clock-independent increases in activity after sudden light-off during
151 the day, flies were repeatedly exposed to a 30-minute dark pulse following 1.5 h of light. The
152 experiments were conducted under "normal day" conditions consisting of 12 h light (30
153 μW/cm^2) and 12 h darkness. The activity data were normalized to account for differences in
154 baseline activity between genotypes. Specifically, the mean activity during all light phases was
155 calculated, excluding time points corresponding to the dark pulses. Each data point was then
156 divided by this genotype-specific average to obtain normalized activity values. For all
157 experimental conditions, data from four consecutive days were averaged, omitting the first day
158 to reduce effects of acclimatization.

159 For the startle response assay (4-hour assay), flies were rendered arrhythmic by exposure to
160 constant light (130 μW/cm^2 ~500 lux) for two days. They were then exposed to repeated 4-
161 hour light-dark cycles, each consisting of 3.5 hours of light (30 μW/cm^2) followed by 30 minutes
162 of darkness, repeated six times per day, for a total duration of three days. Startle activity was
163 recorded during each cycle. Values from all cycles across the three days were averaged, with
164 the first cycle excluded to avoid carryover effects from the prior light regime. Since each light
165 phase lasted 210 minutes, data were plotted with the 30-minute dark pulse centered on the

166 time axis, resulting in two light periods of 105 minutes each, before and after the dark pulse.
167 For normalization, the mean activity during the 105 minutes preceding light-off was set to one,
168 and activity after light-off was expressed relative to this baseline.

169 3.4 Fly lines, Primers, and Antibodies

170 The lines listed below were used for the experiments in this study. To minimize background
171 effects, all lines were previously brought on the same X chromosomal background derived
172 from the control fly CS having a y^+ and w^+ genotype.

173 *Table 1 Fly lines*

Name	Genotype	Comment
WT controls (wild-type controls)	+;+;+	Strain CantonS (CS) (Horn et al., 2019)
Rh7^0	+;+;*Rh7*^{0}	From Kistenpfennig et al. (2017) crossed into the y^+w^+ (CS) background.
Rh7^{MiMIC}	+;+;*Rh7*^{MiMIC}	From Kistenpfennig et al. (2017) crossed into the y^+w^+ (CS) background.
per^{01}	*per*^{01};+;+	From Konopka and Benzer (1971)
per^{01};;*Rh7*^{0}	*per*^{01};+; *Rh7*^{0}	Double mutants carrying the mutations *period*^{01} and *Rh7*^{0}
Rh7-Gal4	+;*Rh7-Gal4*	Extended *Rh7* promoter (8,2kB) construct, spanning ~1kb upstream of transcription start, extending to exon 2 incl. ATG, cloned into *pPTGAL* (Sharma et al., 2002) vector; injected by TheBestGene.
Rh7-Gal4; Rh7^0	+;*Rh7-Gal4; Rh7*^{0}	*Rh7-Gal4* line crossed into *Rh7*^{0} backgound.
UAS-empty / UAS- ()	+; *UAS-empty;Rh7*^{0}	An empty *pUASTattB* (Bischof et al., 2007) construct, with the UAS-backbone and mini-white, CytoSite 2R, 55C4, injected by TheBestGene, crossed into *Rh7*^{0} backgound.
UAS-Rh7	+;*UAS-Rh7;Rh7*^{0}	*Rh7* under UAS control, generated with the *pUASTattB* (Bischof et al., 2007) vector, CytoSite 2R, 55C4, injected by TheBestGene, crossed into *Rh7*^{0} backgound.
UAS-Rh7^{Darkfly}	+;*UAS-Rh7*^{Darkfly};*Rh7*^{0}	*Rh7* lacking the last 21 amino acids, under UAS control, generated with the *pUASTattB* (Bischof et al., 2007) vector, CytoSite 2R, 55C4, injected by TheBestGene, crossed into *Rh7*^{0} backgound.
UAS-GFP-JFRC81	+;*UAS-GFP;*+	*JFRC81-10xUAS-IVS-Syn21-GFP-p10* (Pfeiffer et al., 2012)
UAS-MCFO	see Nern et al. (2015)	Bloomington *Drosophila* Stock Center #64091 (Nern et al., 2015)
Darkfly	see Izutsu et al. (2012)	Kindly provided from Naoyuki Fuse (Izutsu et al., 2012)

174

175

176 *Table 2 Primers*

Application	Name	Sequence (5'-3')
Gal4 driver construct	Rh7 Gal4 Eco52 (1)-5'	CGGCCGTAGTTCATGACGATGCCAGACCAG
	Rh7 Gal4 EcoRI (1)-3'	GACAAGCACGTGAATGACAGCGTTTC
	Rh7 Gal4 EcoRI (2)-5'	CAATCTGGCCTGAATAAAGCCACGG
	Rh7 Gal4 SpeI (2)-3'	AGGCCGTTCACTAGTGAGCACTAC
	Rh7 Gal4 SpeI (3)-5'	GCGGCCGCACGAGTCTAAGTGATGGGTTCCG
	Rh7 Gal4 BglII (3)-3'	CGGGTTTGGCAGAATTTGAAGATCTG
	Rh7 Gal4 BglII (4)-5'	AGTTTCGCAGTGGAAAAGCACTTGC
	Rh7 Gal4 KpnI (4)-3'	GGTACCGATGGCCTCCATGACTGACTTG
UAS construct	UAS-Rh7-5'	CAAGGAATTCATGGAGGCCATCATCATGACGAC
	UAS-Rh7-3'	GTCAGATCTCAGAACTTACTCTGTTCCATGACG
	UAS-Darkfly-3'	CAAAGATCTACTCGTTCTCCTCCGTCTCCTCG
qPCR	Rh7 qPCR-5'	AATCATCCGCTGTGAATGTAGGCAAG
	Rh7 qPCR-3'	AATCAGGAAGGTGCTCGACTTAGGTG
	alphaTub-5'	TCTGCGATTCGATGGTGCCCTTAAC
	alphaTub-3'	GGATCGCACTTGACCATCTGGTTGGC

177

178 *Table 3 Antibodies used for immunohistochemistry*

Application	Antibody	Dilution	Source / Reference
Rh7-Gal4 > UAS-GFP	chicken anti-GFP	1:1000	Rockland, Limerick, PA, USA
	goat anti-chicken Alexa Flour® 488	1:400	Thermo Fischer Scientific
MultiColor FlpOut	chicken Anti-V5	1:100	Fortis Life Sciences
	rabbit anti-OLLAS	1:500	Thermo Fischer Scientific
	rat anti-HA	1:100	Roche
	goat anti- FLAG	1:500	Bethyl Laboratories
	donkey anti-chicken Alexa Flour® 488	1:400	Thermo Fischer Scientific
	donkey anti-rat Alexa Flour® 555	1:400	Thermo Fischer Scientific
	donkey anti-goat Alexa Flour® 594	1:400	Thermo Fischer Scientific
	donkey anti-rabbit Alexa Flour® 680	1:400	Thermo Fischer Scientific

179

180 3.5 Generating the *Rh7-Gal4* line

181 The *Rh7* promoter construct comprised 1,080 bp upstream of exon 1 extending into exon 2,
182 including the translation start site located in exon 2. Due to the overall length of the target
183 region (>8,000 bp), the construct was assembled in four fragments, which were sequentially
184 cloned into the *pPTGAL* vector (Sharma et al., 2002). The four inserts were amplified from *D.*
185 *melanogaster* genomic DNA using specific *Gal4* primer pairs (see Table 2). Insert 1 and insert
186 4 included artificial restriction sites (Eco52 and KpnI, respectively), while all other restriction
187 sites were naturally occurring. Cloning began with insert 4 (see Supplementary Material S2B)
188 and proceeded stepwise with the remaining fragments. Final plasmids were amplified in *E. coli*

189 NEB 10-beta and the construct integrity was confirmed by sequencing. The plasmid was
190 injected into w^{1118} flies by TheBestGene Inc., and the resulting transgenic line was backcrossed
191 into the same $y^{+}w^{+}$ background as the controls.

192 3.6 Generating UAS-constructs

193 For the rescue experiments, a *UAS-Rh7* construct and a *UAS-empty* (*UAS- ()*) construct were
194 generated as controls. The *Rh7* construct was prepared from the *D. melanogaster* cDNA using
195 the primers UAS-Rh7-5' and UAS-Rh7-3' (Table 2), digested with EcoRI and BglII enzymes
196 and ligated into the *pUASTattB* vector (Bischof et al., 2007). For the *UAS-empty* construct, the
197 *pUASTattB* vector was used unmodified. The vectors were then injected into flies with CytoSite
198 2R, 55C4 by the company TheBestGene Inc. All lines were brought into a $+;+;Rh7^{0}$ background
199 and finally crossed with flies with respective *Gal4*-constructs in $+;+;Rh7^{0}$ background and
200 assayed. The $UAS\text{-}Rh7^{Darkfly}$ construct was prepared with the primers UAS-Rh7-5' and UAS-
201 Darkfly-3' (Table 2) with the same steps described above. All transgenic lines were
202 backcrossed into the same $y^{+}w^{+}$ background as the controls.

203 3.7 Optomotor response

204 Male flies were individually tested for their optomotor walking behavior. The setup comprised:
205 (1) an upright cylinder (ø 8 cm; H 4.5 cm) with vertical black and white stripes (2.2 cm width
206 and 4 cm height) inside for visual stimulation and (2) a transparent Plexiglas arena (ø 3 cm; H
207 1.5 cm) with a tube for inserting the flies. Although the arena was 1.5 cm high, the open space
208 available for movement was only about 2 mm, limiting the flies to a single horizontal walking
209 plane (Supplementary Material S2C). The LED-lit cylinder with 6 white and 6 black stripes
210 rotated clockwise (CW) and counterclockwise (CCW) at 16 rpm, equivalent to a frequency of
211 1.6 Hz. The flies had a 2-minute acclimatization without light, followed by 2 minutes under CW
212 rotation with light, a 1-minute rest, and then 2 minutes under CCW rotation with light. For the
213 optomotor response (OR), the number of full circles walked and complete self-turns in the
214 direction of the pattern movement within the two 2 minutes were added, while movements in
215 the opposite direction were subtracted. The result was then divided by the total number of
216 cylinder rotations (4x16).

217 3.8 qPCR

218 For quantitative PCR (qPCR), total RNA was extracted from either five heads, five brains, 10
219 retinas or 10 laminas of control flies. Total RNA was extracted using the Quick-RNA™
220 Microprep Kit (Zymo), and cDNA was synthesized with the QuantiTect Reverse Transcription
221 Kit (Qiagen). For qPCR, three biological replicates were applied for each tissue, with two
222 technical replicates. qPCRs were performed using the SensiFAST™ SYBR® No-ROX Kit
223 (Bioline) in the Qiagen Rotor-Gene Q qPCR machine, with raw data fit by dynamic tube and

224 slope correction calculation using the Rotor-Gene Q Series software. Relative mRNA levels
225 were calculated using the Δ-CT equation, with *α-tubulin* used as a reference gene. qPCR was
226 performed with *Rh7* (Rh7 qPCR-5', Rh7 qPCR-3') and control (alphaTub-5', alphaTub-3')
227 primers, each at 0.1 mM (Table 2).

228 3.9 Immunohistochemistry

229 Fluorescent immunohistochemistry was performed on 3- to 5-day-old male flies. Whole flies
230 were fixed for 3 h in 4% paraformaldehyde in 0.5% PBST (1xPBS with 0.5%Triton X-100)
231 followed by three 10-minute rinses with PBS. The brains were dissected in 0.5% PBST and
232 incubated overnight at 4 °C with 5% normal goat serum (NGS) or normal donkey serum (NDS)
233 and 0.02% NaN_3 in 0.5% PBST, depending on the host species of the secondary antibodies.
234 Antibody solutions contained the antibody in the concentration specified in Table 3 and 5%
235 NGS or NDS with 0.02% NaN_3 in 0.5% PBST. The brains were incubated for two days at 4 °C
236 in primary antibody solution followed by five 10-minute washes with 0.5% PBST. Subsequently,
237 the brains were incubated for at least 4 hours at room temperature or overnight at 4 °C with
238 the secondary antibody solution containing the corresponding secondary antibodies (Table 3).
239 The samples were washed five times for 10 minutes with 0.5% PBST before embedding in
240 VectaShield 1000 mounting medium (Vector Laboratories, Burlingame, CA, USA) using object
241 slides with spacers (~170 µm). The high-precision coverslips (170 ± 5 µm, No.1.5H) were
242 sealed with FixoGum. Brains with retinas attached were embedded with retinas facing the
243 object slide to ensure easy imaging from the posterior. Object slides were stored in the dark at
244 4 °C until scanning. In addition, individual neurons were visualized using the MultiColor FlpOut
245 (MCFO) technique (Nern et al., 2015), which stochastically labels single cells with distinct
246 membrane-targeted fluorescent tags. Flippase-mediated excision of FRT-flanked stop
247 cassettes enables sparse and color-resolved labeling, allowing detailed analysis of neuronal
248 shape and projections. Labeled brains were processed and mounted as described above.

249 3.10 *In situ* hybridization

250 For RNA *in situ* hybridization, we used the hybridization chain reaction v3 (HCR) method
251 developed by Molecular Instruments (Choi et al., 2018). The flies were fixed and dissected as
252 described for the fluorescent immunohistochemistry. The tissue was either used directly for *in*
253 *situ* hybridization or dehydrated and stored in 99% methanol at -20 °C for up to 14 days.
254 Dehydration was performed by sequential incubation in 30%, 50%, 70% and 90% methanol in
255 PBS (2 minutes each). Rehydration was performed in the opposite order. *In situ* HCR was
256 performed using a modified protocol from Bruce et al.(Bruce et al., 2021). In short, *Rh7* probe
257 mixes containing 20 probe pairs were designed by Molecular Instruments. Instead of using
258 Proteinase K or detergent-based solutions, tissues were incubated in 0.5% PBST for 30
259 minutes. This was followed by a 30-minute incubation at 37 °C in preheated probe hybridization

260 buffer (Molecular Instruments), and then an overnight incubation (≥20 h) at 37 °C in preheated
261 probe hybridization buffer containing the *Rh7* probe mix (12 nM). After hybridization the tissue
262 was washed four times for 15 minutes each with preheated probe washing buffer (Molecular
263 instruments) at 37 °C. This was followed by two washes at room temperature (5 minutes each)
264 in 5xSSCT (5xSSC buffer with 1% Tween20). Next, the tissues were incubated for 30 minutes
265 at room temperature in amplification buffer (Molecular Instruments) followed by incubation for
266 at least 20 h at room temperature in amplification buffer containing the hairpins required for
267 signal amplification. Hairpins were prepared by heating 3 µM h1 hairpins and 3 µM h2 hairpins
268 separately in amplification buffer to 95 °C for 90 seconds. They were then cooled to room
269 temperature for 30 minutes, protected from light, before being mixed and applied to the tissue.
270 When hairpins were reused, the already mixed hairpins were reheated together. After five
271 washes with 5x SSCT (2 x 5 minutes, 3 x 30 minutes) the tissues were either directly embedded
272 in VectaShield as described above, or the normal fluorescent immunohistochemistry protocol
273 was used for additional antibody labeling starting with blocking in 5% NGS or NDS.

274 3.11 Image acquisition and analysis

275 Images were acquired with a Leica TCS SP8 confocal microscope equipped with a photon
276 multiplier tube and hybrid detector. A white light laser (Leica Microsystems, Wetzlar, Germany)
277 was used for excitation. We used a 20-fold glycerol immersion objective (0.73 NA, HC PL APO,
278 Leica Microsystems, Wetzlar Germany) for wholemount scans. We obtained 8-bit confocal
279 stacks with 2048 × 1024 pixels with a maximal voxel size of 0.3 x 0.3 x 2 µm and an optical
280 section thickness of 3.12 µm. Weak signals were amplified using line accumulation. Images
281 were analyzed using Fiji. No changes in pixel intensity were applied other than linear changes
282 in brightness and contrast.

283 4 Results

284 4.1 Phylogenetic and functional distinction of RH7 from other r-opsins

285 To determine the time of origin of RH7 and other r-opsins, a phylogenetic tree was carried out.
286 This analysis clearly identifies the three clades of *Drosophila* rhodopsins including the RH7
287 clade (Figure 2A). While RH1, RH2, and RH6 form the first rhodopsin clade (Figure 2A, blue),
288 which seems to be more distinct from the RH7 clade, the clade formed by RH3, RH4, and RH5
289 (Figure 2A, magenta) is more closely related to RH7. In contrast to the other two clades that
290 include only rhodopsin homologues of other arthropods, the RH7 clade also includes
291 homologues from Onychophora (*Euperipatoides kanangrensis*) and Tardigrada (e.g. *Hypsibius*
292 *dujardini*). Rhodopsin sequences of other arthropods that are not related to *Drosophila*
293 rhodopsins are shown in gray (Figure 2A). The detailed tree in higher resolution can be found

in Supplementary Materials S3. The presence of RH7 in Tardigrada and Onychophora, unlike other rhodopsins, indicates an early origin within panarthropods (Figure 2B).

To test the functionality of RH7, we used a GsX assay designed to determine which G_α proteins can bind to a given GPCR, in this case RH7 (Ballister et al., 2018). This assay employs chimeric G_α proteins that share a core derived from G_αs, which triggers cAMP production upon activation. The C terminal 14 amino acids of each chimera, critical for GPCR binding, are replaced with sequences from other G_α subtypes, such as G_αq or G_αz. This allows each chimera to mimic the coupling specificity of a distinct G protein while ensuring that any productive GPCR interaction results in a measurable increase in cAMP levels. For this analysis, we co-expressed RH7 with various GsX chimeras in HEK cells and stimulated RH7 with brief light pulses. We observed robust activation with the G_αz chimera, regardless of whether 9-cis-retinal or all-trans-retinal was present (Figure 2C). Although there is no G_αz homolog in *Drosophila*, related G_α subunits such as G_αo and G_αi are expressed in the fly. Nevertheless, these results revealed two key findings: (1) RH7 can be activated by light, and (2) RH7 does not appear to signal via the G_αq-mediated pathway, unlike other *Drosophila* rhodopsins. These findings indicate that RH7 exhibits a signaling profile distinct from other insect rhodopsins.

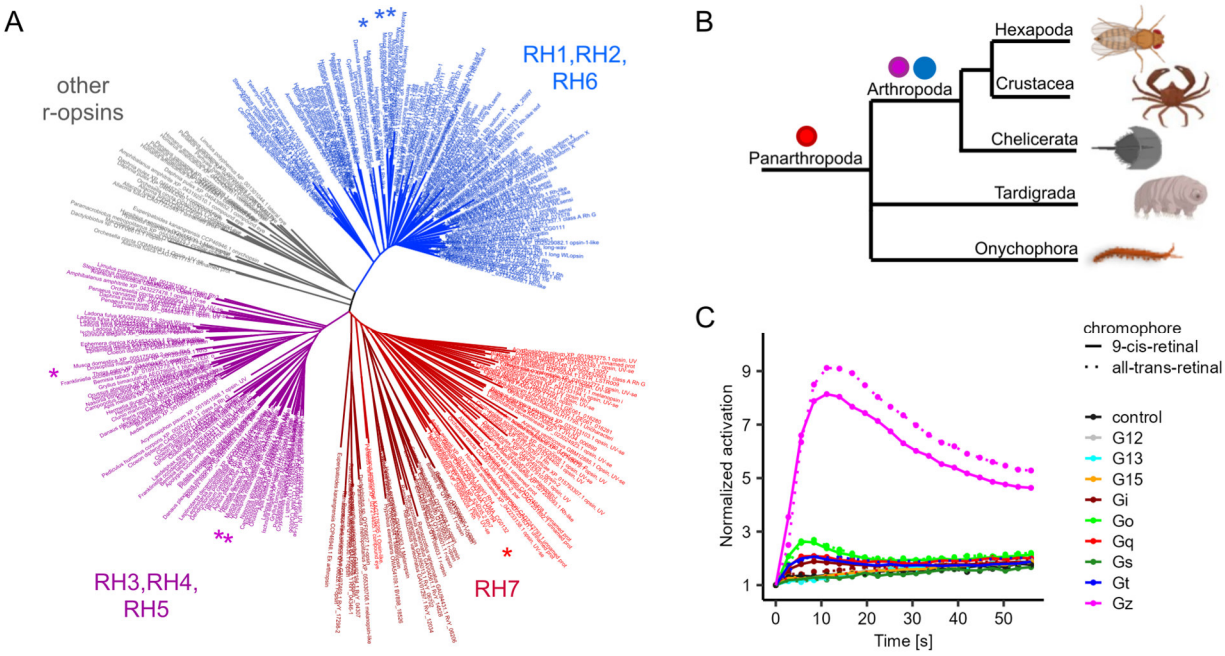

Figure 2 A) Phylogenetic tree of 280 r-opsin proteins, highlighting the clades containing Drosophila rhodopsins: RH1, RH2, and RH6 (blue); RH3, RH4, and RH5 (purple); and RH7 (red/dark red). Arthropod RH7 homologs are shown in red, while homologs from tardigrades and onychophorans are shown in dark red. Drosophila rhodopsins are marked with stars in their respective clade colors. B) Proposed evolutionary timeline of Drosophila rhodopsins. RH7 likely emerged in the last common ancestor of panarthropods (red circle), while the other two rhodopsin clades evolved later within arthropods (purple and blue circles). C) GsX assay showing that RH7 robustly activates the G_αz chimera in a light-dependent manner, with minimal differences between 9-cis-retinal and all-trans-retinal. No activation was detected with the G_αq chimera.

4.2 *Rh7⁰* mutants show decreased activity during darkness

To study the influence of RH7 on the daily activity of flies, wild-type (WT) control flies and *Rh7⁰* mutants were examined under different light conditions. We found significant differences in activity profiles between the mutants and controls on standard 12-hour light/dark cycles (LD 12:12) (Figure 3A). During the day, mutants and wild-type controls showed the morning and evening activity typical of *Drosophila melanogaster* with a siesta in between. Even though the overall activity of the flies remained the same throughout the day, *Rh7⁰* mutants were clearly less active during the night and compensated for this deficit with increased daytime activity (Figure 3A*). The startle response after light-off, a brief activity burst lasting 5-10 minutes, was greatly reduced in *Rh7⁰* mutants. Daily temperature fluctuations (29 °C day, 24 °C night) further amplified the difference between *Rh7⁰* mutants and wild-type controls. Under these conditions, control flies shifted their activity to the cooler dark phase, while *Rh7⁰* mutants showed only a slight shift. After light-off, *Rh7⁰* mutants quickly reduced activity and entered the resting phase, whereas wild-type controls remained active longer (Figure 3B, B*). Under short day conditions (LD 8:16), wild-type control flies strongly shifted their activity to the dark phase, while *Rh7⁰* mutants showed a weaker shift (Figure 3C, C*).

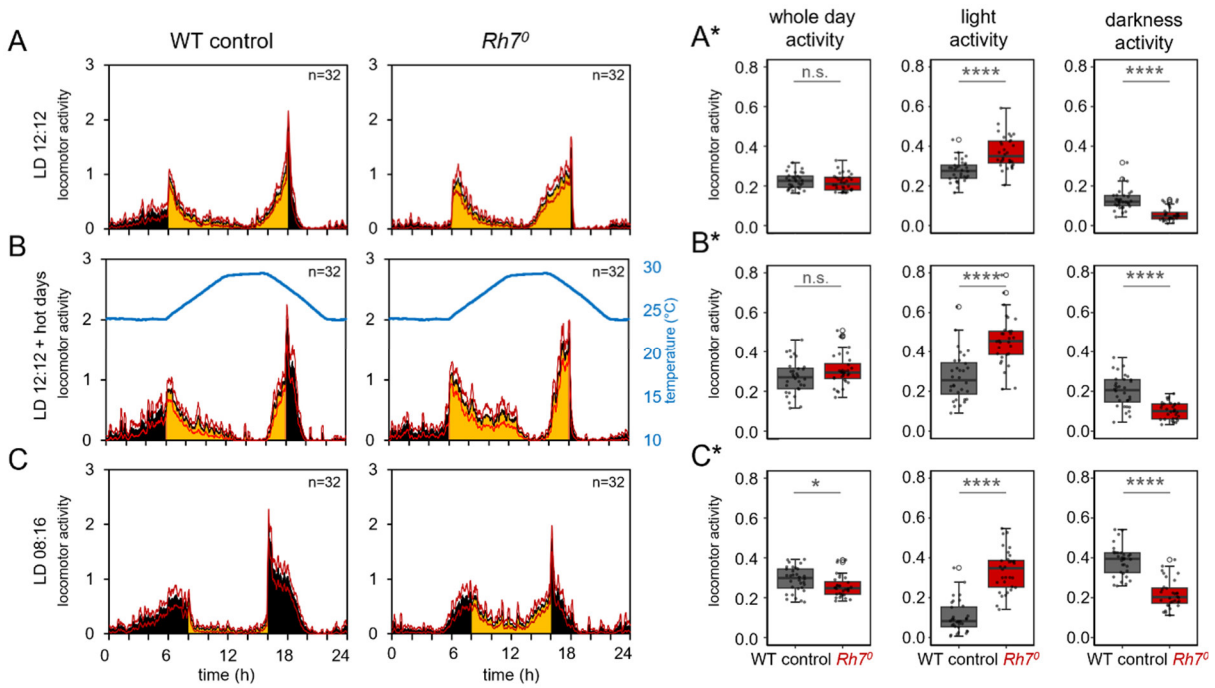

Figure 3 Rh7⁰ mutants show reduced activity in the dark. Average activity profiles of wild-type (WT) control flies and Rh7⁰ mutants are shown for A) "normal days" (12 h light (30 µW/cm²): 12 h dark, 25 °C), B) "hot days" (12 h light (30 µW/cm²): 12 h dark, 24-29 °C), and C) "short days" (8 h light (30 µW/cm²) : 16 h dark, 25 °C). Wild-type control flies exhibit anticipatory activity in the morning and a short startle response in the evening, both are reduced in Rh7⁰ mutants. On "short" and "hot" days, control flies shift more activity to the dark phase, while Rh7⁰ mutants remain mainly active in the light phase. A, B*, and C* show total activity and activity in light and dark phases. Total activity is similar on "normal" and "hot days", but Rh7⁰ mutants are less active on "short days". Rh7⁰ mutants are significantly more active in the light phase and less active in the dark phase than wild-type controls (****p <0.0001, *p <0.05, Mann-Whitney U-Test, R-studio).*

346 ### 4.3 Startle response to light-off persists without a functional clock

347 The startle response, triggered by the sudden light-off, differs from circadian-regulated evening
348 activity and can occur during the day as well. To test the startle response, we performed 30-
349 minute dark pulses every 1.5 hours during the light phase on a standard LD 12:12 day and
350 recorded fly activity. We observed that the startle responses of both wild-type controls and
351 mutants were generally lower in the morning than in the afternoon (Figure 4A). The circadian
352 clock and thus the internal state of flies appear to influence the startle response, as can be
353 seen in clockless per^{01} mutants. Per^{01} mutants exhibited a startle response that remains
354 constant throughout the day. This startle response is significantly and consistently reduced in
355 the per^{01};;$Rh7^{0}$ double mutants (Figure 4A). These results show that the startle response is
356 influenced by the circadian clock but functions independently, with RH7 playing a key role.

357 To focus solely on the startle response and exclude any circadian clock effects, flies were
358 rendered arrhythmic by exposing them to continuous bright light (130 μW/cm^2) for two days.
359 This led to sustained activation of the blue light receptor *Drosophila* type CRYPTOCHROME
360 (DCRY or CRY) and continuous degradation of TIMELESS, resulting in a standstill of the
361 molecular clock (Deppisch et al., 2022; Dolezelova et al., 2007; Emery et al., 2000). The light
362 was then switched off for 30 minutes every 3.5 hours for three days (4-hour assay). To quantify
363 the behavioral response, startle reactions were normalized as described above and averaged
364 across trials within each genotype. Under these conditions, $Rh7^{0}$ mutants exhibited
365 significantly reduced startle responses compared to wild-type controls (Figure 4B, top row).
366 Notably, $Rh7^{MiMIC}$ mutants, previously examined by Kistenpfennig et al.(Kistenpfennig et al.,
367 2017) displayed a similar phenotype. qPCR analysis revealed that $Rh7^{MiMIC}$ mutants retain
368 reduced but detectable mRNA levels, indicating an additional *Rh7* mutant line with altered gene
369 expression, while $Rh7^{0}$ mutants completely lack *Rh7* transcripts (Supplementary Material
370 S2D). This phenotype remained when the two alleles ($Rh7^{0}$ and $Rh7^{MiMIC}$) were tested in trans
371 to each other but disappeared in heterozygous *x/+* flies, confirming the critical role of RH7 in
372 mediating the startle response (Figure 4B, bottom row).

373 ### 4.4 Rh7 is expressed in the optic lobe and clock neurons

374 To determine the tissue-specific expression of *Rh7*, we performed qPCR analyses using α-
375 *tubulin* as a reference gene. The expression of *Rh7* was highest in the lamina, followed by the
376 brain, while only minimal levels were detected in the retina (Figure 5A). Additionally, we
377 performed *Rh7* RNA *in situ* hybridization chain reaction (HCR), which verified the strongest
378 *Rh7* expression in the lamina and medulla (Figure 5B). We further observed considerably
379 weaker expressions in neurons of the central brain (Figure 5B). No *in situ* hybridization was
380 detected in $Rh7^{0}$ mutants (Figure 5C).

381

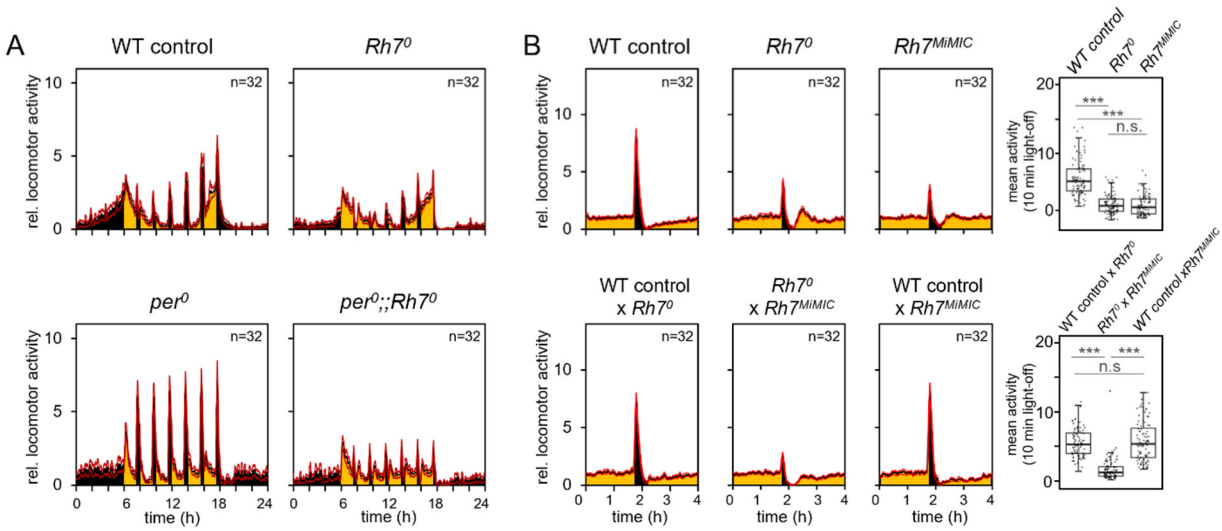

*Figure 4 A) The average daily activity of fly strains was recorded under a 12 h light (30 µW/cm²) : 12 h dark cycle at 25 °C. During the light phase, the light was turned off for 0.5 h every 1.5 h to observe the startle response to light-off. To compare fly lines with different baseline activity, activity was normalized to their light-phase activity. All fly strains show a startle response to each dark pulse, but this is reduced in $Rh7^0$ and per^{01};;$Rh7^0$ mutants. The light-off startle response varies by time of day but stays constant in per^0 and per^0;;$Rh7^0$ mutants. B) The startle response 4-hour assay. WT controls, as well as the heterozygous flies crossed with $Rh7^0$ or $Rh7^{MiMIC}$, show a strong startle response which is characterized by a short-term increase in activity. In the homozygous $Rh7^0$ and $Rh7^{MiMIC}$ lines, as well as in the line carrying on one chromosome the $Rh7^0$ mutation and on the other the $Rh7^{MiMIC}$ mutation, this startle response is significantly reduced (***p <0.001, Mann-Whitney U-Test, R-studio).*

To further investigate *Rh7* expression, we generated a *Rh7* promoter-driven *Gal4* line (*Rh7-Gal4*). Since the *Rh7* gene expression regulatory elements are not only located within the promoter but also extend into the transcriptional region, we cloned a large part of this region, including exon 1, intron 1 and part of exon 2, together with the start codon (Supplementary Material S2B).

When comparing GFP expression driven by the newly generated *Rh7-Gal4* with the *Rh7* RNA *in situ* hybridization and qPCR data, we again observed the strongest expression in the lamina and medulla. Interestingly, also the *Rh7-Gal4* line showed additional expression in neurons of the central brain (Figure 5D). Some of the stained dorsally located neurons are part of the clock network as can be seen from the colocalization with the antibody against the clock protein PERIOD. This subset of neurons includes some DN_{1p}, DN_{1a}, and DN_2 neurons (Figure 5H). To test whether these clock neurons also express *cry,* we performed simultaneous RNA *in situ* hybridization for *cry and Rh7.* As suggested by single cell RNA sequencing data (Ma et al., 2021; Reinhard et al., 2024), the clock neurons expressing *Rh7* are CRY-negative with the DN_{1a} forming the only exception (Supplementary Material S2E). To validate the expression pattern of the *Rh7-Gal4* line, we performed *in situ* hybridization with *Rh7-Gal4>GFP* flies. All GFP-labeled cells were also detected by RNA *in situ* hybridization, although the signal was less pronounced in cells of the central brain. Some cells, particularly in the optic system, were detected only by *in situ* hybridization and not by the *Gal4* line. This suggests an even broader expression of *Rh7* than shown by the *Gal4* line (Figure 5F, G). To further characterize *Rh7-*

expressing neurons, we used MultiColor FlpOut (MCFO) (Nern et al., 2015), which stochastically labels neurons when crossed to a *Gal4*-driver line. Using MCFO, we identified at least two cell types of the optic system based on their characteristic arborization pattern in the medulla: lamina neuron 5 (L5) and medulla intrinsic neuron 1 Mi1 (Figure 5E). Both neurons were also present in the TAPIN RNA-seq analysis, with L5 showing the strongest *Rh7* expression (Davis et al., 2020).

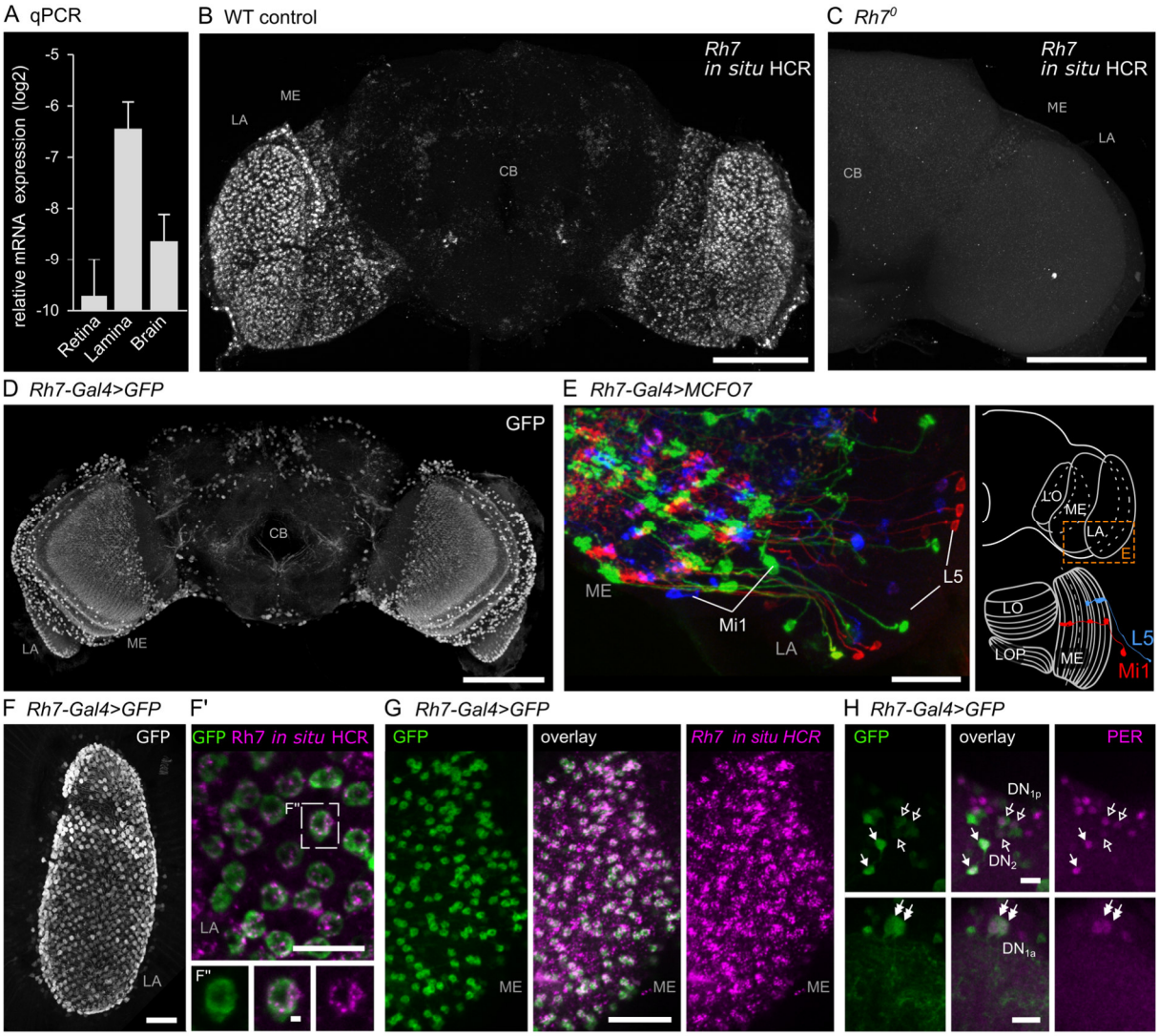

Figure 5 Relative qPCR analysis revealed strong Rh7 expression in the lamina, followed by the brain, with minimal background expression in the retina. B) Rh7 in situ HCR in wild-type (WT) controls revealed strong Rh7 signals in the lamina (LA) and medulla (ME), and weaker signals in the central brain (CB). C) Rh7⁰ mutants showed no detectable Rh7 in situ HCR signal, confirming the specificity of the probe and the loss of Rh7 expression in the mutant. D) Rh7-Gal4-driven UAS-GFP expression revealed robust labeling in the optic system, particularly in the lamina and medulla, as well as in various brain cells. E) Rh7-Gal4-driven MCFO labeling identified lamina neurons L5 and the medulla neuron Mi1. Right: schematic illustration of the detected neurons in the optic lobe. F & G) in situ HCR in Rh7-Gal4>GFP flies revealed that all GFP-labeled cells in the lamina (F) and medulla (G) also showed Rh7 transcript signal, confirming Rh7 expression in these neurons. H) Immunostaining of Rh7-Gal4>UAS-GFP flies with anti-GFP and anti-PER antibodies revealed co-labeling in clock neurons, suggesting that a subset of circadian neurons expresses Rh7. Open arrows mark DN_{1p} and arrows mark DN2; double arrows mark DN_{1a}. Scale bar in B, C, D represents 100 µm, in E, F, G 25 µm, in F', H 10 µm and in F" 1 µm.

431 ### 4.5 C-terminal truncation of RH7 affects dark-phase behavior

432 The so-called Darkfly was kept in complete darkness for 57 years (1400 generations)
433 accumulating mutations that may have enhanced its adaptation to perpetual darkness (Izutsu
434 et al., 2012). Notably, the mutant carries a nonsense mutation in the *Rh7* gene, resulting in the
435 loss of the final 21 amino acids at the C-terminus. qPCR analyses indicate that *Rh7* transcript
436 levels are unchanged, suggesting that the truncated RH7 protein is indeed expressed
437 (Supplementary Material S2D). When we exposed the Darkfly to dark pulses in a 12:12 light-
438 dark cycle, they exhibited the opposite phenotype of $Rh7^0$ mutants, showing a stronger startle
439 response (Figure 6A), possibly reflecting increased RHODOPSIN 7 activity in the Darkfly strain
440 (Figure 6A).

441 To validate the role of *Rh7* in the startle response, we conducted a rescue experiment by re-
442 expressing *Rh7* in $Rh7^0$ mutants using the *UAS-Rh7* construct driven by *Rh7-Gal4*. As a control
443 for cloning and insertion artifacts, we used a *UAS-empty* line with the same insertion site as
444 *UAS-Rh7*, driven by *Rh7-Gal4* in the $Rh7^0$ background. In the dark pulse experiment, *Rh7-*
445 *Gal4>UAS-empty;*$Rh7^0$ flies behaved like mutants, while *Rh7-Gal4>UAS-Rh7;*$Rh7^0$ flies
446 resembled wild-type controls (Figure 6B). To express a truncated RH7 protein lacking the last
447 21 amino acids, as found in the Darkfly, we crossed the *UAS-*$Rh7^{Darkfly}$*;* $Rh7^0$ line with the *Rh7-*
448 *Gal4;* $Rh7^0$ line. We observed an increased startle response in the offspring, most prominently
449 during the second half of the light phase (Figure 6B). In the 4-hour assay, in which the flies
450 were made arrhythmic we found a clear rescue of the startle response in *Rh7-Gal4>UAS-*
451 *Rh7;*$Rh7^0$ flies compared to the *Rh7-Gal4>UAS-empty;*$Rh7^0$ controls. Furthermore, *Rh7-*
452 *Gal4>UAS-*$Rh7^{Darkfly}$*;*$Rh7^0$ flies showed a significantly increased startle response (Figure 6C).

453 ### 4.6 RH7 modulates optomotor responses

454 The *Drosophila* optomotor response is a reflex that stabilizes locomotion by counteracting
455 perceived environmental motion with its own motion. The optic system, particularly the lamina
456 neurons, plays an important role in this response (Yang and Clandinin, 2018). We found that
457 $Rh7^0$ mutants show deficits in the optomotor response, while the Darkfly showed an increased
458 optomotor response (Figure 6D). When the rescue flies were tested, the *Rh7-Gal4>UAS-*
459 *empty;*$Rh7^0$ flies behaved like the $Rh7^0$ mutants, whereas the *Rh7-Gal4>UAS-Rh7;*$Rh7^0$ flies
460 showed a significant rescue, with no significant difference from wild-type controls. In contrast,
461 *Rh7-Gal4>UAS-*$Rh7^{Darkfly}$*;*$Rh7^0$ flies showed a significantly higher optomotor response than the
462 wild-type controls and the *Rh7-Gal4>UAS-Rh7;*$Rh7^0$ flies. This response was similar to the
463 Darkfly (Figure 6E).

464

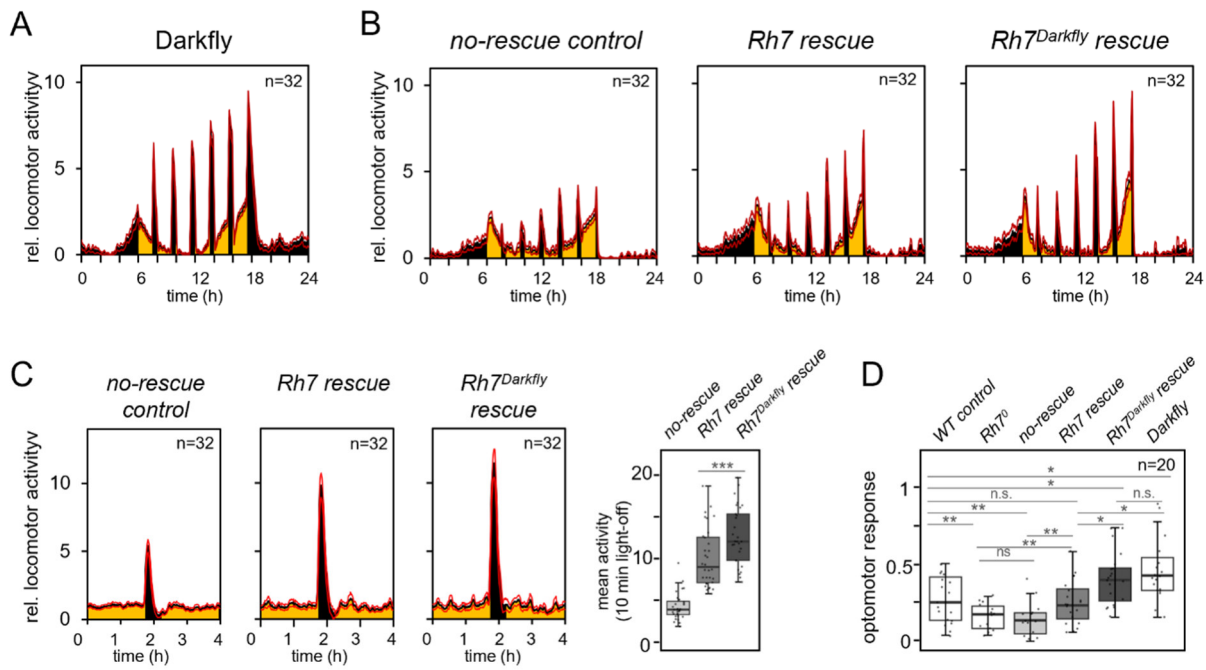

*Figure 6 A & B) Normalized average daily activity of Darkfly and rescue fly lines recorded under a 12 h light (30 µW/cm²) / 12 h dark cycle at 25 °C. During the light phase, lights were turned off for 30 min every 1.5 h. A) Darkfly flies exhibit an enhanced startle response to light-off. B) No-rescue controls (Rh7-Gal4>UAS-empty; Rh7º) display a phenotype similar to Rh7 mutants, whereas the Rh7 rescue line (Rh7-Gal4>UAS-Rh7; Rh7º) resembles WT controls. The Rh7Darkfly (Rh7-Gal4>UAS-Rh7Darkfly; Rh7º) rescue shows an enhanced startle response similar to Darkfly, particularly during the second half of the day. C) To measure the startle response, the 4-hour assay was performed. The Rh7 rescue line restored the reduced startle response seen in the no-rescue controls, which behave like Rh7º mutants ($p < 0.0001$). The Rh7Darkfly rescue showed an even stronger startle response, significantly higher than the Rh7 rescue line ($p < 0.001$). D) Optomotor response assays show that no-rescue controls behave like Rh7º mutants, with no significant difference between them. Rh7 rescue flies respond like WT controls. Both Rh7º mutants and no-rescue controls differ significantly from WT and Rh7 rescue flies ($p < 0.01$). Darkfly and Rh7Darkfly rescue flies do not differ from each other but show significant differences compared to WT and Rh7 rescue flies (***$p < 0.001$, **$p < 0.01$, *$p < 0.05$, Mann-Whitney U-Test).*

5 Discussion

5.1 RH7 is an ancestral and structurally distinct opsin

Although RH7 has been known for nearly 25 years, its function remains poorly understood. This is partly due to its atypical expression outside the retina and its divergence from canonical visual rhodopsins. Phylogenetic analyses indicate that RH7 is the most ancestral opsin within the *Drosophila* genus. Homologs identified in tardigrades and onychophorans (Figure 2A) point to a deep evolutionary origin within Panarthropoda, suggesting that RH7 belongs to an ancient class of opsins (Figure 2B). In onychophorans and tardigrades, two early branching panarthropod groups, RH7-like opsins have been linked to monochromatic vision (Beckmann et al., 2015; Fleming et al., 2021; Hering and Mayer, 2014).

The ancestral character of RH7 is further reflected in its unusual structural features. Unlike other *Drosophila* rhodopsins, RH7 has markedly longer N- and C-terminal regions, which are roughly twice as long and contain a high density of predicted phosphorylation sites. This

suggests a high potential for post-translational regulation and possibly increased signaling flexibility. The extended termini distinguish RH7 from the more compact structure of typical rhodopsins and may represent an intermediate stage between canonical GPCRs and specialized visual rhodopsins (Figure 7A). In addition, RH7 lacks several conserved motifs found in other *Drosophila* rhodopsins, which likely emerged during the specialization of visual opsins. The absence of these features, together with the extended termini, supports the idea that RH7 occupies a structurally and evolutionarily distinct position. A more detailed comparison of these motifs and their functional implications is presented in section 5.5.

Besides its structural divergence, the developmental origin and central localization of RH7-expressing neurons support its ancestral photoreceptive role. RH7 localizes to central visual neuropils such as the lamina and medulla that process input from peripheral photoreceptors. Unlike canonical R-opsins, which are primarily expressed in specialized retinal photoreceptor cells, RH7 expression in central brain regions suggests an ancient form of non-image-forming photoreception integrated directly within neural circuits. This idea is further supported by the presence of opsins expressed in brain regions of other early-diverging bilaterians, such as annelids and mollusks (Arendt et al., 2004; Vöcking et al., 2015; Wollesen et al., 2019). RH7 may thus represent an evolutionarily conserved opsin for central light sensing that predates the functional separation of sensory input and processing centers.

5.2 Divergence from canonical signaling: first insights into RH7 phototransduction

The signaling properties of RH7 were explored using heterologous GsX assays, which clearly indicated that RH7 can be activated by light (Figure 2C) but does not interact with $G_{\alpha}q$. This lack of interaction appears plausible, as $G_{\alpha}q$ expression is restricted to retinal cells, whereas RH7 is expressed in lamina and medulla neurons (Davis et al., 2020). The $G_{\alpha}q$-binding domains are highly conserved between mammals and *Drosophila* (93% identity, Supplementary Material S2F), meaning that RH7 should interact with mammalian $G_{\alpha}q$ if it engages in a $G_{\alpha}q$-mediated signaling pathway. Instead of interacting with $G_{\alpha}q$, RH7 appears to interact with mammalian $G_{\alpha}z$. Although *Drosophila* lacks a direct homolog of $G_{\alpha}z$, the related inhibitory subunits $G_{\alpha}i$ and $G_{\alpha}o$ from the same family may serve as functional analogs.

If RH7 indeed couples to a $G_{\alpha}i$ family member, this would represent a notable exception among *Drosophila* rhodopsins by engaging an inhibitory G protein pathway. This possible reversal of signaling direction recalls the mammalian system, where melanopsin in ipRGCs activates an excitatory $G_{\alpha}q$ pathway, while classical retinal rhodopsin signals through an inhibitory transducin ($G_{\alpha}t$) pathway belonging to the $G_{\alpha}i$ family (Contreras et al., 2021; Gao et al., 2019; Koyanagi and Terakita, 2008). The use of opposing G protein pathways in these systems,

527 despite their evolutionary distance, may reflect a conserved principle that links photoreceptor
528 polarity to downstream signaling.

529 5.3 RH7 in the optic lobe: A modulator of early visual processing

530 *Rh7* is broadly expressed in the optic lobe, particularly in the lamina and medulla, which are
531 key regions for early visual processing. These areas receive input from outer photoreceptors
532 and are involved in contrast and motion detection. We found strong *Rh7* expression in L5
533 lamina neurons and Mi1 neurons of the medulla. L5 neurons pass signals from outer
534 photoreceptors to the medulla, where Mi1 neurons help process motion and contrast
535 information.

536 Our behavioral data support a role for RH7 in modulating these visual functions. Flies lacking
537 *Rh7* show reduced optomotor responses, suggesting they are less sensitive to moving visual
538 stimuli. In contrast, the Darkfly strain, which expresses a truncated variant of RH7, shows an
539 increased response in the same assay (Figure 6D). Rescue experiments confirm that this effect
540 depends on *Rh7*: expression of full-length RH7 in *Rh7*^{o} mutants restores normal behavior,
541 while the truncated form of the Darkfly enhances the optomotor response. These results
542 indicate that RH7 influences visual processing in the optic lobe. The enhanced behavior seen
543 with the Darkfly variant suggests that changes in RH7 structure can affect its function. This
544 possibility is discussed further in section 5.5.

545 5.4 RH7 in circadian regulation and behavioral flexibility

546 Fly activity is shaped by both the circadian clock and external light cues, which are detected
547 by specialized photoreceptors. In *Drosophila*, RH7 contributes to this light-dependent
548 regulation. Under standard 12:12 light-dark cycles, *Drosophila melanogaster* displays two
549 peaks of locomotor activity in the morning and evening separated by a midday siesta (Helfrich-
550 Förster, 2000). This rhythm is controlled by the circadian clock and its associated neuronal
551 network. Flies experience two rest phases: a pronounced one at night and a shorter one during
552 the siesta, both primarily regulated by dorsal clock neurons (DNs) (Guo et al., 2018). The DN_1
553 subclass plays a key sleep-promoting role and includes CRY-positive and CRY-negative
554 neurons that may contribute differently to the two rest phases (Guo et al., 2016; Lamaze and
555 Stanewsky, 2020).

556 Although *Drosophila* is generally active during the light phase, activity can shift into the dark
557 phase under specific conditions such as heat stress or short photoperiods. This behavioral
558 flexibility is reduced in *Rh7*^{o} mutants. They show decreased night activity and fail to adjust their
559 behavior to darkness, pointing to a role for RH7 in conveying light input to the circadian system
560 (Figure 3). Daily activity levels remain similar between mutants and wild-type controls,

561 suggesting that these effects reflect changes in circadian regulation rather than general
562 locomotor impairment.

563 RH7 is expressed in dorsal clock neurons, especially in CRY-negative DN_1, with the exception
564 of the two DN_{1a} neurons (Figure 5H). Notably, nearly all sequenced species that possess RH7
565 also contain DCRY (Deppisch et al., 2023; Senthilan and Helfrich-Förster, 2016), suggesting
566 a potential functional interplay between these two photoreceptors within the circadian light
567 input network.

568 While we could confirm RH7 expression in the dorsal clock neurons, we did not detect it in
569 lateral clock neurons (Figure 5B, D), as previously suggested by Ni et al. (Ni et al., 2017). This
570 finding is consistent with findings reported in Senthilan et al. (Senthilan et al., 2019). In addition
571 to its role in dorsal neurons, RH7 may also influence circadian regulation via the optic lobe. Its
572 expression in the lamina and medulla, along with possible synaptic connections between Mi1
573 neurons and PDF-expressing neurons (Reinhard et al., 2024), and the presence of PDF
574 receptors in lamina neurons (Bastian et al., 2025; Davis et al., 2020), suggest a functional link
575 between early visual processing centers and the circadian network.

576 **5.5** **RH7 is essential for locomotor activity during darkness**

577 Although activity during darkness is regulated by the circadian clock, the startle response to
578 light-off is independent of it. Dark-pulse experiments show that both wild-type controls and *per*^{o}
579 mutants, which lack a functional circadian clock, exhibit a strong startle response. While the
580 circadian clock seems to influence the magnitude of the response, it is not essential for its
581 occurrence (Figure 4A). Moreover, this phenotype persists in flies rendered arrhythmic during
582 the 4-hour assay. The critical role of RH7 is supported by trans-heterozygous combinations
583 with *Rh7*^{MiMIC}, which show the same phenotype as *Rh7*^{o} mutants, and by rescue experiments
584 restoring normal behavior (Figure 4B).

585 The Darkfly strain, bred in complete darkness for many generations, provides an intriguing
586 case for RH7 function in sustained darkness. It carries an RH7 variant with a 21-amino acid
587 deletion in the C-terminal tail, a region rich in predicted phosphorylation sites. Structural
588 modeling based on AlphaFold predicts an interaction between this tail and the receptor core,
589 specifically the unique ICL3 loop of RH7 (Figure 1A, Supplementary Material S2A), which lacks
590 the QAKKMNV motif found in other *Drosophila* rhodopsins. Such intramolecular interactions
591 are known to mediate autoinhibition in GPCRs, where the C-terminal tail stabilizes an inactive
592 conformation that shifts to an active state upon receptor stimulation (Maggio et al., 2023).

593 We hypothesize that the deletion in the Darkfly variant weakens this autoinhibitory interaction
594 and thus facilitates constitutive activation (Figure 7B). This is supported by the observation that
595 deleting the final 21 amino acids increases dark-phase activity and optomotor response,

596 approaching levels seen in Darkfly flies (Figure 6). However, while the RH7 mutation largely
597 accounts for the increased dark activity, the enhanced phenotype in the Darkfly strain likely
598 reflects the combined effects of additional mutations accumulated during long-term dark
599 rearing (Izutsu et al., 2012), which may also influence neural development or synaptic
600 connectivity. Overall, these findings highlight the pivotal role of RH7 in modulating behavior in
601 darkness and demonstrate that structural changes can fine-tune RH7 signaling to adapt to
602 environmental conditions.

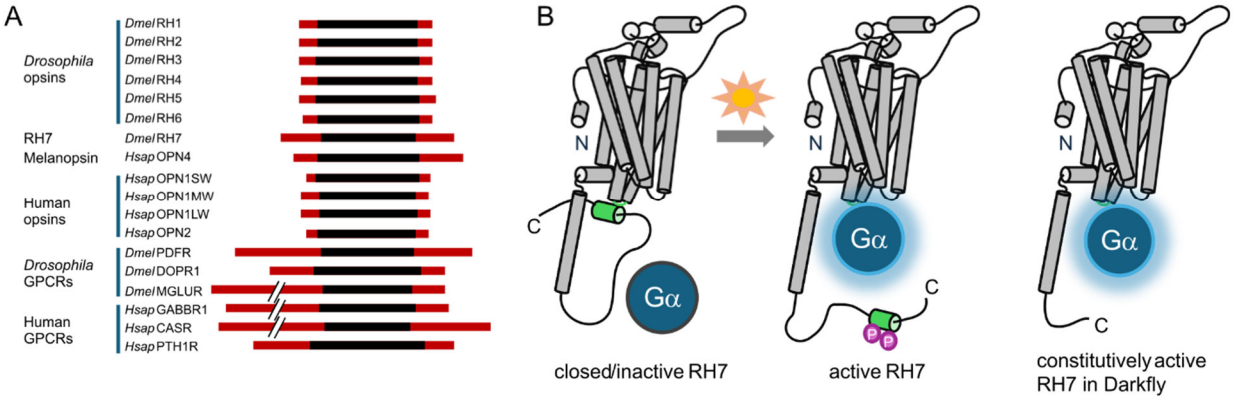

603

604 *Figure 7 A) Protein lengths of Drosophila and human opsins are shown alongside randomly selected non-opsin*
605 *GPCRs. General GPCRs are significantly longer, primarily due to extended N- and C-termini, whereas opsins are*
606 *shorter and largely confined to the transmembrane core. RH7 and OPN4 (melanopsin) display intermediate protein*
607 *lengths relative to both groups. The red bars represent the N- and C-termini of the proteins, and the black bars*
608 *represent the core protein, spanning from the 1st to the 7th transmembrane domain. Additional information,*
609 *including full protein names and UniProt IDs, is provided in Supplementary Material S2G. B) Left: Predicted 3D*
610 *structure of RH7 based on AlphaFold, representing a closed conformation. Center: A putative open conformation*
611 *that may result from light-induced conformational changes and subsequent C-terminal phosphorylation (magenta),*
612 *potentially promoting G-protein binding, as suggested by Maggio et al. (Maggio et al., 2023). Right: Hypothetical*
613 *structure of RH7 in the Darkfly variant, possibly stabilized in an open, constitutively active state, independent of*
614 *light.*

615 **5.6 Parallels and divergence between *Drosophila* RH7 and other**
616 **noncanonical Opsins**

617 This study highlights significant similarities between RH7 and other noncanonical rhodopsins,
618 particularly mammalian melanopsin (OPN4). Both RH7 and melanopsin are expressed in
619 neurons downstream of classical photoreceptors, with RH7 in lamina and medulla neurons of
620 the optic lobe and melanopsin in the ipRGCs, suggesting analogous roles in processing visual
621 and circadian information. Functionally, both opsins contribute to circadian regulation as well
622 as contrast and motion detection. Structurally, they share elongated N- and C-terminal regions
623 that are intermediate in length relative to canonical rhodopsins and typical GPCRs. These
624 extended regions harbor multiple phosphorylation sites likely crucial for their unique signaling
625 mechanisms.

626 Furthermore, RH7 and melanopsin activate phototransduction cascades distinct from those of
627 classical visual opsins, potentially producing opposing effects. This reflects an evolutionary

adaptation that supports diverse functions in both visual and nonvisual photoreception. However, while melanopsin expression in mammals is largely confined to the visual system, *Drosophila* RH7 appears to have acquired additional functions in the brain. This divergence may reflect evolutionary adaptations to differing anatomical constraints: the small, light-permeable brain of *Drosophila* may permit direct light sensing beyond the eyes, whereas in mammals, the evolution of a larger brain enclosed by a light-impermeable skull may have limited such extraocular photoreception to specialized retinal pathways.

Although melanopsin is predominantly expressed in retinal ganglion cells, it has also been detected in various brain regions (Aviles-Trigueros et al., 2012; Nissilä et al., 2017). Additionally, other non-canonical opsins such as encephalopsin and neuropsin are present in the human brain, with their functional roles still under investigation (Buhr et al., 2015; Nissilä et al., 2012; Upton et al., 2022, 2021). In this context, the expression of RH7 in the *Drosophila* brain, outside of clock neurons, may reflect similar non-visual roles. While its brain expression is relatively weak compared to its prominent presence in the optic lobes, it is consistently observed using both *Rh7-Gal4* reporters and *in situ* hybridization. The identity of the non-clock neuronal populations expressing *Rh*7 remains to be determined, and further work, such as double labeling with cell-type-specific markers, will be necessary to clarify this. In these neurons, RH7 might contribute to higher-order visual processing, sensorimotor control, general arousal, or aspects of neuronal development.

These findings open new possibilities to study how noncanonical opsins like RH7 contribute to complex brain functions beyond just sensing light. Understanding the roles of RH7 can give important clues about how light-sensing systems evolved and how they work together with brain circuits to control behavior. Future research using genetics, anatomy, and physiology will be important to fully understand all the functions of RH7 in *Drosophila* and other animals.

6 Conclusion

Our study provides a key insight into the unresolved functional diversity of opsins. Unlike canonical rhodopsins involved in image formation, RH7 acts as a fundamental photoreceptor mediating simple light-on and light-off signals to diverse neuronal populations. As an evolutionarily ancient opsin, RH7 likely represents a primordial photoreceptive system predating the specialization of complex visual pathways. Structurally and functionally, RH7 exhibits characteristic features of G protein-coupled receptors (GPCRs), positioning it as an evolutionary intermediate between ancestral GPCRs and specialized visual opsins. This is reflected in its atypical sequence motifs, extended terminal domains, and distinct signaling properties, which collectively blur the distinction between classical visual and non-visual photoreception.

Functionally, RH7 modulates early visual processing in the lamina and might contribute to circadian regulation in dorsal clock neurons. Its phylogenetic and mechanistic parallels to mammalian melanopsin further support its role as a GPCR-like photoreceptor integrating environmental light cues with intracellular signaling cascades to regulate physiology and behavior. In summary, RH7 exemplifies how ancient opsins have diversified to couple photoreception with GPCR-mediated signaling beyond image formation. Its expression in brain regions highlights a conserved evolutionary strategy: the integration of light sensitivity into central neural circuits, underscoring the deep-rooted link between sensory and neurodevelopmental architectures.

7 Resource availability

All data supporting this study are available within the main text or the Supplemental Information. Additional details can be obtained from the corresponding author upon request.

8 Acknowledgements

We thank Kathrin Sauter, Christina Brunner, and Marina Müller for technical assistance. We also acknowledge Maria Gallant and Barbara Mühlbauer for their support, and Giulia Manoli for help with data analysis. We are grateful to Naoyuki Fuse for providing Darkfly, to E. Kostenis and A. Inoue for the HEK293ΔG7 cell line, and to Martin Göpfert and Marion Silies for valuable discussions. This work was supported by the German Research Foundation (DFG), SE 2320/1-1, SO 1337/2-2, and the DFG Heisenberg program SO 1337/6-1.

9 Author contributions

V.K. performed fly activity assays, optomotor experiments, generated UAS-construct lines, and carried out MCFO stainings and qPCR analyses. N.R. performed immunohistochemistry and in situ hybridizations. H.H. generated the *Rh7-Gal4* line. A.M. contributed additional fly activity assays. D.R. established experimental setups and contributed to experimental design. P.S. carried out the GsX assay. C.H.-F. contributed to conceptual discussions, provided critical input throughout the project, and performed dissections for qPCR. P.R.S. designed the experiments, coordinated the study, analyzed experimental results, performed phylogenetic analyses, and wrote the manuscript. All authors reviewed and approved the final manuscript.

10 Declaration of interests

The authors declare no competing interests.

11 Declaration of generative AI and AI-assisted technologies in the writing process

During the preparation of this work the authors used DeepL and ChatGPT in order to improve the readability and language of the manuscript. After using these tools, the authors reviewed and edited the content as needed and take full responsibility for the content of the published article.

12 References

Arendt D, Tessmar-Raible K, Snyman H, Dorresteijn AW, Wittbrodt J. 2004. Ciliary Photoreceptors with a Vertebrate-Type Opsin in an Invertebrate Brain. *Science* **306**:869–871. doi:10.1126/science.1099955

Aviles-Trigueros M, Matínez-Garrido F, Nadal-Nicolás F, Agudo-Barriuso M, Selles-Navarro I, Vidal-Sanz M. 2012. Melanopsin-like Photopigment Expression In Adult Mammal Brain. *Investigative Ophthalmology & Visual Science* **53**:4336.

Ballister ER, Rodgers J, Martial F, Lucas RJ. 2018. A live cell assay of GPCR coupling allows identification of optogenetic tools for controlling Go and Gi signaling. *BMC Biology* **16**:10. doi:10.1186/s12915-017-0475-2

Bastian FB, Cammarata AB, Carsanaro S, Detering H, Huang W-T, Joye S, Niknejad A, Nyamari M, Mendes de Farias T, Moretti S, Tzivanopoulou M, Wollbrett J, Robinson-Rechavi M. 2025. Bgee in 2024: focus on curated single-cell RNA-seq datasets, and query tools. *Nucleic Acids Research* **53**:D878–D885. doi:10.1093/nar/gkae1118

Beckmann H, Hering L, Henze MJ, Kelber A, Stevenson PA, Mayer G. 2015. Spectral sensitivity in Onychophora (velvet worms) revealed by electroretinograms, phototactic behaviour and opsin gene expression. *J Exp Biol* **218**:915–922. doi:10.1242/jeb.116780

Bischof J, Maeda RK, Hediger M, Karch F, Basler K. 2007. An optimized transgenesis system for Drosophila using germ-line-specific φC31 integrases. *Proceedings of the National Academy of Sciences* **104**:3312–3317. doi:10.1073/pnas.0611511104

Bowin C-F, Inoue A, Schulte G. 2019. WNT-3A-induced β-catenin signaling does not require signaling through heterotrimeric G proteins. *J Biol Chem* **294**:11677–11684. doi:10.1074/jbc.AC119.009412

Bruce HS, Jerz G, Kelly S, McCarthy J, Pomerantz A, Senevirathne G, Sherrard A, Sun DA, Wolff C, Patel NH. 2021. Hybridization Chain Reaction (HCR) In Situ Protocol.

Buhr ED, Yue WWS, Ren X, Jiang Z, Liao H-WR, Mei X, Vemaraju S, Nguyen M-T, Reed RR, Lang RA, Yau K-W, Van Gelder RN. 2015. Neuropsin (OPN5)-mediated photoentrainment of local circadian oscillators in mammalian retina and cornea. *Proc Natl Acad Sci U S A* **112**:13093–13098. doi:10.1073/pnas.1516259112

Choi HMT, Schwarzkopf M, Fornace ME, Acharya A, Artavanis G, Stegmaier J, Cunha A, Pierce NA. 2018. Third-generation in situ hybridization chain reaction: multiplexed, quantitative, sensitive, versatile, robust. *Development* **145**:dev165753. doi:10.1242/dev.165753

Contreras E, Nobleman AP, Robinson PR, Schmidt TM. 2021. Melanopsin phototransduction: beyond canonical cascades. *J Exp Biol* **224**:jeb226522. doi:10.1242/jeb.226522

Datta RR, Rister J. 2022. The power of the (imperfect) palindrome: Sequence-specific roles of palindromic motifs in gene regulation. *Bioessays* **44**:e2100191. doi:10.1002/bies.202100191

Davis FP, Nern A, Picard S, Reiser MB, Rubin GM, Eddy SR, Henry GL. 2020. A genetic, genomic, and computational resource for exploring neural circuit function. *eLife* **9**:e50901. doi:10.7554/eLife.50901

Deppisch P, Helfrich-Förster C, Senthilan PR. 2022. The Gain and Loss of Cryptochrome/Photolyase Family Members during Evolution. *Genes* **13**:1613. doi:10.3390/genes13091613

Deppisch P, Kirsch V, Helfrich-Förster C, Senthilan PR. 2023. Contribution of cryptochromes and photolyases for insect life under sunlight. *J Comp Physiol A* **209**:373–389. doi:10.1007/s00359-022-01607-5

Dolezelova E, Dolezel D, Hall JC. 2007. Rhythm Defects Caused by Newly Engineered Null Mutations in Drosophila's cryptochrome Gene. *Genetics* **177**:329–345. doi:10.1534/genetics.107.076513

Emery P, Stanewsky R, Hall JC, Rosbash M. 2000. A unique circadian-rhythm photoreceptor. *Nature* **404**:456–457. doi:10.1038/35006558

Feuda R, Marlétaz F, Bentley MA, Holland PWH. 2016. Conservation, Duplication, and Divergence of Five Opsin Genes in Insect Evolution. *Genome Biol Evol* **8**:579–587. doi:10.1093/gbe/evw015

Fleming JF, Pisani D, Arakawa K. 2021. New Tardigrade Opsins and Differential Expression Analyses Show Ontogenic Variation in Light Perception. *Genome Biol Evol* **13**:evab164. doi:10.1093/gbe/evab164

Gao Y, Hu H, Ramachandran S, Erickson JW, Cerione RA, Skiniotis G. 2019. Structures of the Rhodopsin-Transducin Complex: Insights into G Protein Activation. *Mol Cell* **75**:781-790.e3. doi:10.1016/j.molcel.2019.06.007

Grebler R, Kistenpfennig C, Rieger D, Bentrop J, Schneuwly S, Senthilan PR, Helfrich-Förster C. 2017. Drosophila Rhodopsin 7 can partially replace the structural role of Rhodopsin 1, but not its physiological function. *J Comp Physiol A* **203**:649–659. doi:10.1007/s00359-017-1182-8

Guo F, Holla M, Díaz MM, Rosbash M. 2018. A Circadian Output Circuit Controls Sleep-Wake Arousal in Drosophila. *Neuron* **100**:624-635.e4. doi:10.1016/j.neuron.2018.09.002

Guo F, Yu J, Jung HJ, Abruzzi KC, Luo W, Griffith LC, Rosbash M. 2016. Circadian neuron feedback controls the Drosophila sleep--activity profile. *Nature* **536**:292–297. doi:10.1038/nature19097

Helfrich-Förster C. 2000. Differential control of morning and evening components in the activity rhythm of Drosophila melanogaster--sex-specific differences suggest a different quality of activity. *J Biol Rhythms* **15**:135–154. doi:10.1177/074873040001500208

Hering L, Mayer G. 2014. Analysis of the Opsin Repertoire in the Tardigrade Hypsibius dujardini Provides Insights into the Evolution of Opsin Genes in Panarthropoda. *Genome Biol Evol* **6**:2380–2391. doi:10.1093/gbe/evu193

Horn M, Mitesser O, Hovestadt T, Yoshii T, Rieger D, Helfrich-Förster C. 2019. The Circadian Clock Improves Fitness in the Fruit Fly, Drosophila melanogaster. *Front Physiol* **10**. doi:10.3389/fphys.2019.01374

Izutsu M, Zhou J, Sugiyama Y, Nishimura O, Aizu T, Toyoda A, Fujiyama A, Agata K, Fuse N. 2012. Genome Features of "Dark-Fly", a Drosophila Line Reared Long-Term in a Dark Environment. *PLoS One* **7**:e33288. doi:10.1371/journal.pone.0033288

Jumper J, Evans R, Pritzel A, Green T, Figurnov M, Ronneberger O, Tunyasuvunakool K, Bates R, Žídek A, Potapenko A, Bridgland A, Meyer C, Kohl SAA, Ballard AJ, Cowie A, Romera-Paredes B, Nikolov S, Jain R, Adler J, Back T, Petersen S, Reiman D, Clancy E, Zielinski M, Steinegger M, Pacholska M, Berghammer T, Bodenstein S, Silver D, Vinyals O, Senior AW, Kavukcuoglu K, Kohli P, Hassabis D. 2021. Highly accurate protein structure prediction with AlphaFold. *Nature* **596**:583–589. doi:10.1038/s41586-021-03819-2

Kingston ACN, Cronin TW. 2016. Diverse Distributions of Extraocular Opsins in Crustaceans, Cephalopods, and Fish. *Integrative and Comparative Biology* **56**:820–833. doi:10.1093/icb/icw022

Kistenpfennig C, Grebler R, Ogueta M, Hermann-Luibl C, Schlichting M, Stanewsky R, Senthilan PR, Helfrich-Förster C. 2017. A New Rhodopsin Influences Light-dependent Daily Activity Patterns of Fruit Flies. *J Biol Rhythms* **32**:406–422. doi:10.1177/0748730417721826

Konopka RJ, Benzer S. 1971. Clock Mutants of Drosophila melanogaster. *Proc Natl Acad Sci U S A* **68**:2112–2116.

Koyanagi M, Terakita A. 2008. Gq-coupled Rhodopsin Subfamily Composed of Invertebrate Visual Pigment and Melanopsin. *Photochemistry and Photobiology* **84**:1024–1030. doi:10.1111/j.1751-1097.2008.00369.x

Lamaze A, Stanewsky R. 2020. DN1p or the “Fluffy” Cerberus of Clock Outputs. *Front Physiol* **10**. doi:10.3389/fphys.2019.01540

Leung NY, Montell C. 2017. Unconventional Roles of Opsins. *Annu Rev Cell Dev Biol* **33**:241–264. doi:10.1146/annurev-cellbio-100616-060432

Leung NY, Thakur DP, Gurav AS, Kim SH, Di Pizio A, Niv MY, Montell C. 2020. Functions of Opsins in Drosophila Taste. *Curr Biol* **30**:1367-1379.e6. doi:10.1016/j.cub.2020.01.068

Ma D, Przybylski D, Abruzzi KC, Schlichting M, Li Q, Long X, Rosbash M. 2021. A transcriptomic taxonomy of Drosophila circadian neurons around the clock. *eLife* **10**:e63056. doi:10.7554/eLife.63056

Maggio R, Fasciani I, Petragnano F, Coppolino MF, Scarselli M, Rossi M. 2023. Unraveling the Functional Significance of Unstructured Regions in G Protein-Coupled Receptors. *Biomolecules* **13**:1431. doi:10.3390/biom13101431

Nern A, Pfeiffer BD, Rubin GM. 2015. Optimized tools for multicolor stochastic labeling reveal diverse stereotyped cell arrangements in the fly visual system. *Proc Natl Acad Sci U S A* **112**:E2967–E2976. doi:10.1073/pnas.1506763112

Ni JD, Baik LS, Holmes TC, Montell C. 2017. A rhodopsin in the brain functions in circadian photoentrainment in Drosophila. *Nature* **545**:340–344. doi:10.1038/nature22325

Nissilä J, Mänttäri S, Särkioja T, Tuominen H, Takala T, Timonen M, Saarela S. 2012. Encephalopsin (OPN3) protein abundance in the adult mouse brain. *J Comp Physiol A Neuroethol Sens Neural Behav Physiol* **198**:833–839. doi:10.1007/s00359-012-0754-x

Nissilä JS, Mänttäri SK, Särkioja TT, Tuominen HJ, Takala TE, Kiviniemi VJ, Sormunen RT, Saarela SYO, Timonen MJ. 2017. The distribution of melanopsin (OPN4) protein in the human brain. *Chronobiol Int* **34**:37–44. doi:10.1080/07420528.2016.1232269

Pfeiffer BD, Truman JW, Rubin GM. 2012. Using translational enhancers to increase transgene expression in Drosophila. *Proc Natl Acad Sci U S A* **109**:6626–6631. doi:10.1073/pnas.1204520109

Reinhard N, Fukuda A, Manoli G, Derksen E, Saito A, Möller G, Sekiguchi M, Rieger D, Helfrich-Förster C, Yoshii T, Zandawala M. 2024. Synaptic connectome of the Drosophila circadian clock. *Nat Commun* **15**:10392. doi:10.1038/s41467-024-54694-0

Rister J, Razzaq A, Boodram P, Desai N, Tsanis C, Chen H, Jukam D, Desplan C. 2015. Single base pair differences in a shared motif determine differential Rhodopsin expression. *Science* **350**:1258–1261. doi:10.1126/science.aab3417

Senthilan PR, Grebler R, Reinhard N, Rieger D, Helfrich-Förster C. 2019. Role of Rhodopsins as Circadian Photoreceptors in the Drosophila melanogaster. *Biology* **8**:6. doi:10.3390/biology8010006

Senthilan PR, Helfrich-Förster C. 2016. Rhodopsin 7–The unusual Rhodopsin in Drosophila. *PeerJ* **4**:e2427. doi:10.7717/peerj.2427

Senthilan PR, Piepenbrock D, Ovezmyradov G, Nadrowski B, Bechstedt S, Pauls S, Winkler M, Möbius W, Howard J, Göpfert MC. 2012. Drosophila auditory organ genes and genetic hearing defects. *Cell* **150**:1042–1054. doi:10.1016/j.cell.2012.06.043

Sharma Y, Cheung U, Larsen EW, Eberl DF. 2002. PPTGAL, a convenient Gal4 P-element vector for testing expression of enhancer fragments in drosophila. *genesis* **34**:115–118. doi:10.1002/gene.10127

Shen WL, Kwon Y, Adegbola AA, Luo J, Chess A, Montell C. 2011. Function of rhodopsin in temperature discrimination in Drosophila. *Science* **331**:1333–1336. doi:10.1126/science.1198904

Sonoda T, Lee SK, Birnbaumer L, Schmidt TM. 2018. Melanopsin Phototransduction Is Repurposed by ipRGC Subtypes to Shape the Function of Distinct Visual Circuits. *Neuron* **99**:754-767.e4. doi:10.1016/j.neuron.2018.06.032

Terakita A. 2005. The opsins. *Genome Biology* **6**:213. doi:10.1186/gb-2005-6-3-213

Upton BA, Díaz NM, Gordon SA, Van Gelder RN, Buhr ED, Lang RA. 2021. Evolutionary Constraint on Visual and Nonvisual Mammalian Opsins. *J Biol Rhythms* **36**:109–126. doi:10.1177/0748730421999870

Upton BA, Nayak G, Schweinzger I, D'Souza SP, Vorhees CV, Williams MT, Earl BR, Lang RA. 2022. Comprehensive Behavioral Analysis of Opsin 3 (Encephalopsin)-Deficient Mice Identifies Role in Modulation of Acoustic Startle Reflex. *eNeuro* **9**. doi:10.1523/ENEURO.0202-22.2022

Vöcking O, Kourtesis I, Hausen H. 2015. Posterior eyespots in larval chitons have a molecular identity similar to anterior cerebral eyes in other bilaterians. *EvoDevo* **6**:40. doi:10.1186/s13227-015-0036-0

Wollesen T, McDougall C, Arendt D. 2019. Remnants of ancestral larval eyes in an eyeless mollusk? Molecular characterization of photoreceptors in the scaphopod Antalis entalis. *EvoDevo* **10**:25. doi:10.1186/s13227-019-0140-7

Xiong B, Bellen HJ. 2013. Rhodopsin homeostasis and retinal degeneration: lessons from the fly. *Trends in Neurosciences* **36**:652–660. doi:10.1016/j.tins.2013.08.003

Yang HH, Clandinin TR. 2018. Elementary Motion Detection in Drosophila: Algorithms and Mechanisms. *Annual Review of Vision Science* **4**:143–163. doi:10.1146/annurev-vision-091517-034153

Zanini D, Giraldo D, Warren B, Katana R, Andrés M, Reddy S, Pauls S, Schwedhelm-Domeyer N, Geurten BRH, Göpfert MC. 2018. Proprioceptive Opsin Functions in Drosophila Larval Locomotion. *Neuron* **98**:67-74.e4. doi:10.1016/j.neuron.2018.02.028

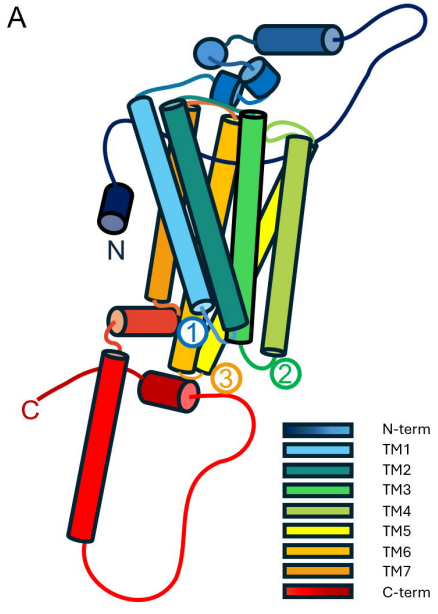
A
N
C
1
2
3
N-term
TM1
TM2
TM3
TM4
TM5
TM6
TM7
C-term

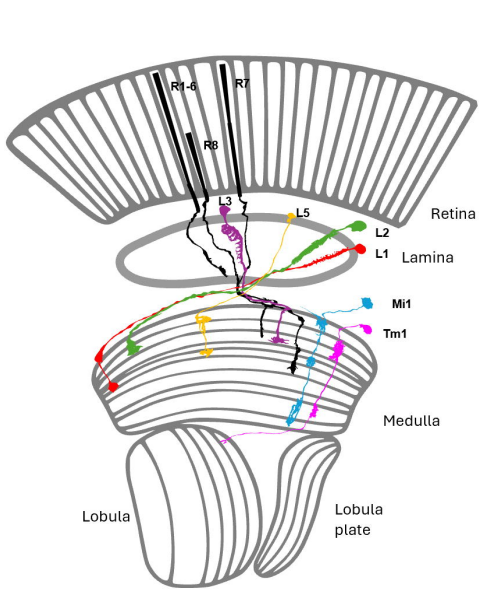
B
R1-6
R7
R8
L3
L5
L2
L1
Retina
Lamina
Mi1
Tm1
Medulla
Lobula
Lobula plate

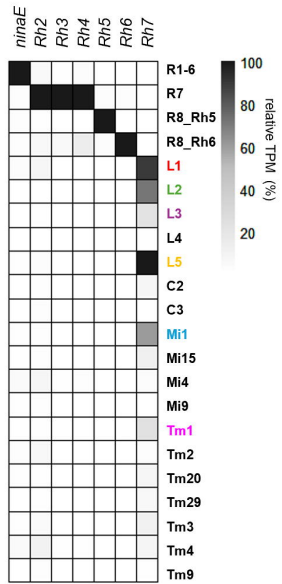
ninaE
Rh2
Rh3
Rh4
Rh5
Rh6
Rh7
R1-6
R7
R8_Rh5
R8_Rh6
L1
L2
L3
L4
L5
C2
C3
Mi1
Mi15
Mi4
Mi9
Tm1
Tm2
Tm20
Tm29
Tm3
Tm4
Tm9
100
80
60
40
20
relative TPM (%)

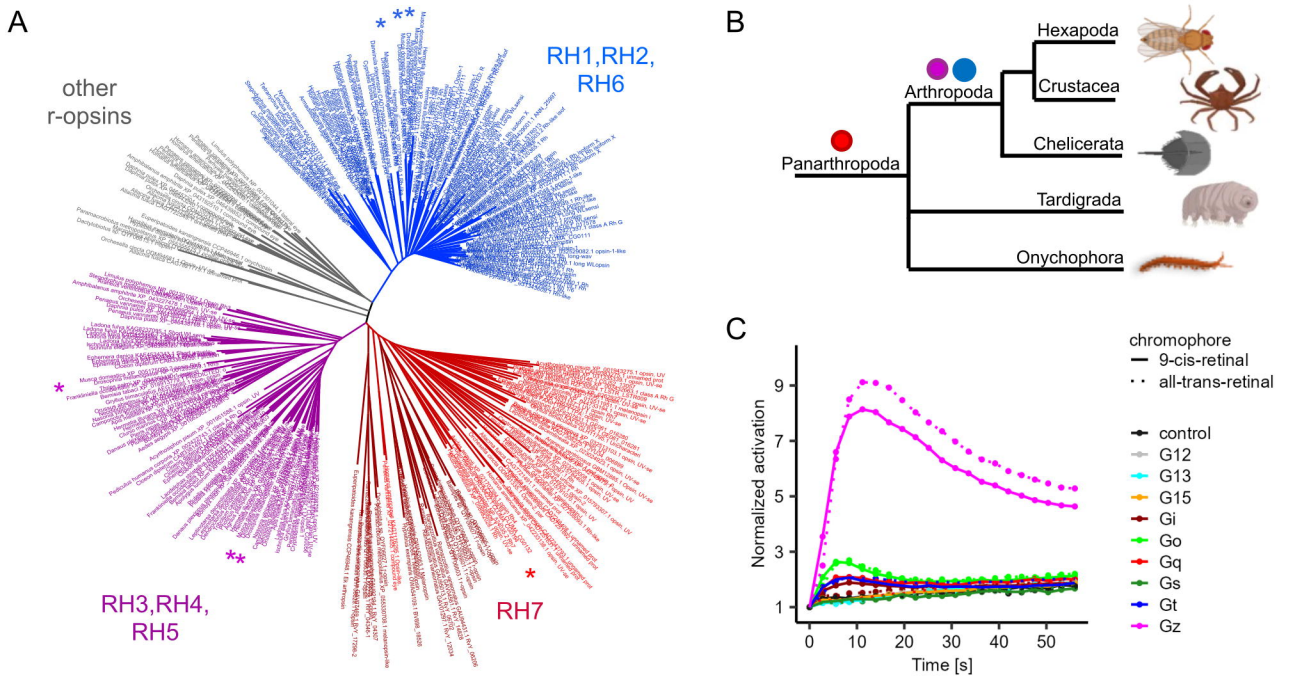
A
other
r-opsins
RH1,RH2,
RH6
RH3,RH4,
RH5
RH7
B
Hexapoda
Crustacea
Arthropoda
Chelicerata
Panarthropoda
Tardigrada
Onychophora
C
chromophore
9-cis-retinal
all-trans-retinal
control
G12
G13
G15
Gi
Go
Gq
Gs
Gt
Gz
Normalized activation
Time [s]

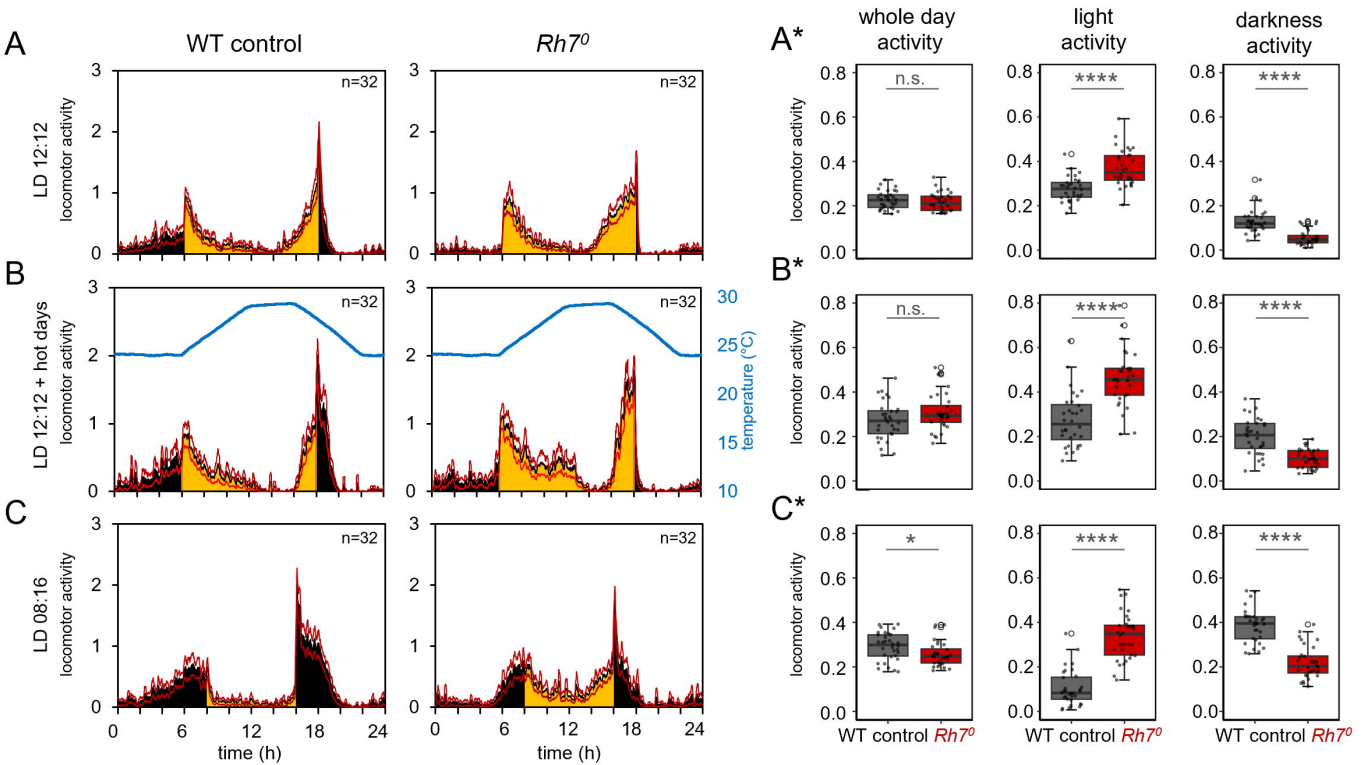
A
WT control
Rh7⁰
n=32
LD 12:12
locomotor activity
B
LD 12:12 + hot days
temperature (°C)
C
LD 08:16
time (h)
A*
B*
C*
whole day activity
light activity
darkness activity
n.s.
****
*
WT control
Rh7⁰

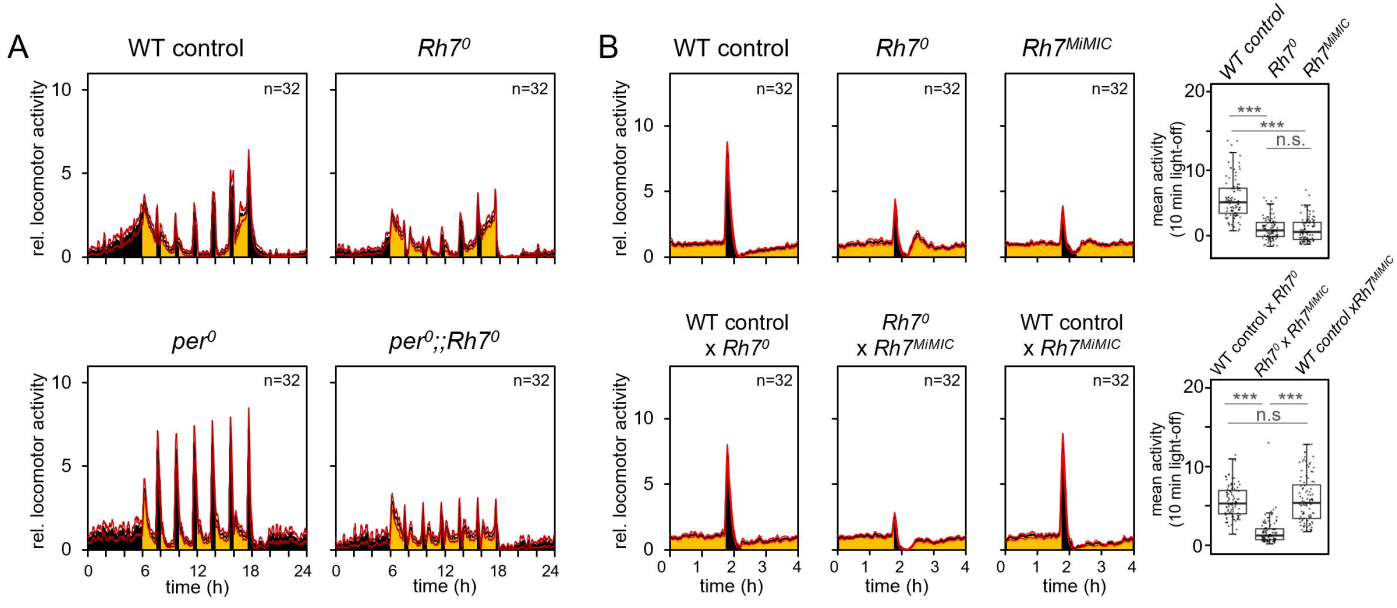
A
WT control
Rh7⁰
per⁰
per⁰;;Rh7⁰
n=32
rel. locomotor activity
time (h)
B
WT control
Rh7⁰
Rh7MiMIC
WT control x Rh7⁰
Rh7⁰ x Rh7MiMIC
WT control x Rh7MiMIC
mean activity (10 min light-off)
***
n.s.
n.s

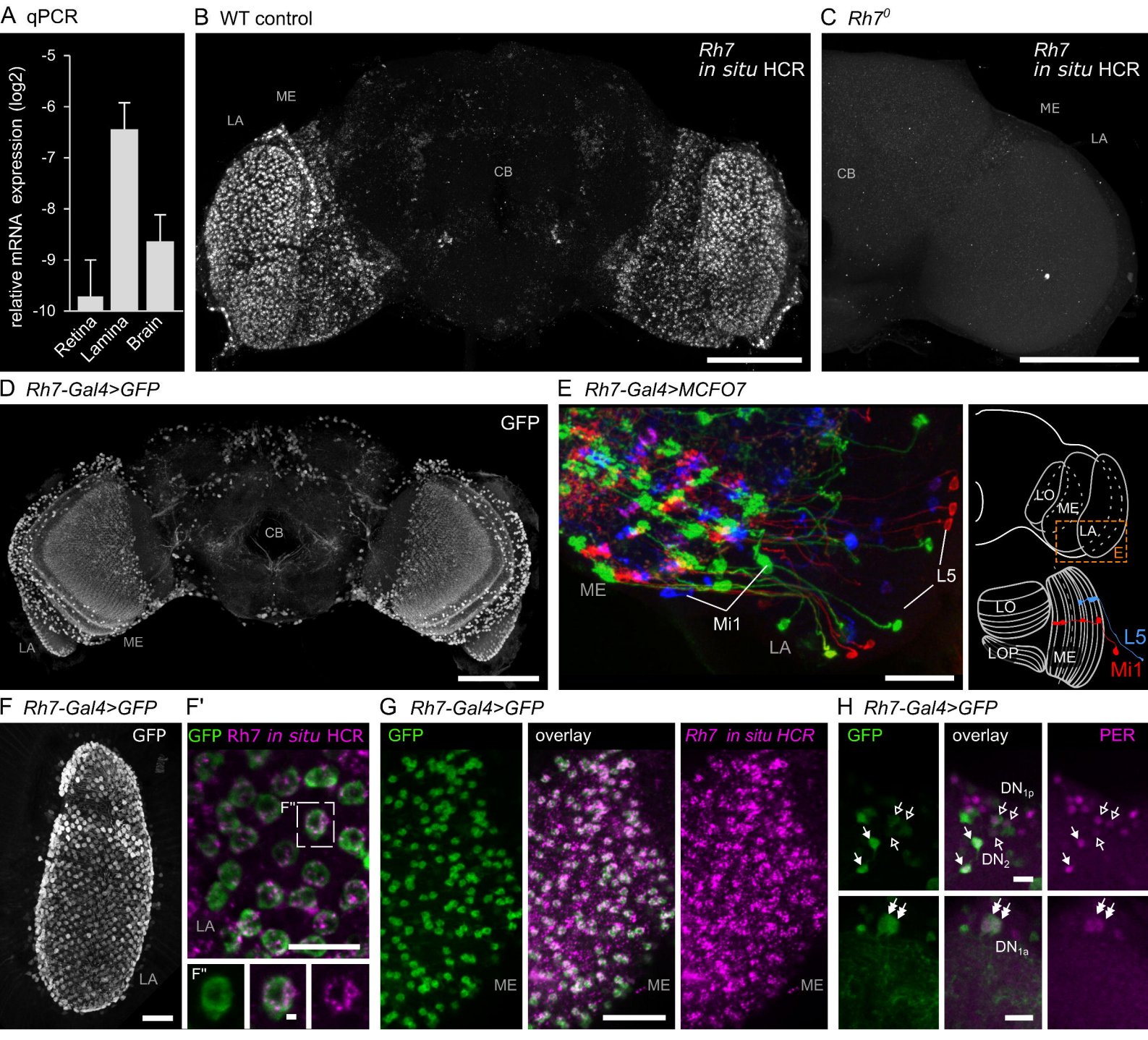
A qPCR
relative mRNA expression (log2)
-5
-6
-7
-8
-9
-10
Retina
Lamina
Brain
B WT control
Rh7
in situ HCR
ME
LA
CB
C Rh7⁰
Rh7
in situ HCR
ME
LA
CB
D Rh7-Gal4>GFP
GFP
CB
LA
ME
E Rh7-Gal4>MCFO7
ME
Mi1
LA
L5
LO
ME
LA
E
LO
LOP
ME
L5
Mi1
F Rh7-Gal4>GFP
GFP
LA
F'
GFP Rh7 in situ HCR
F''
LA
F''
G Rh7-Gal4>GFP
GFP
ME
overlay
ME
Rh7 in situ HCR
ME
H Rh7-Gal4>GFP
GFP
overlay
PER
DN1p
DN2
DN1a

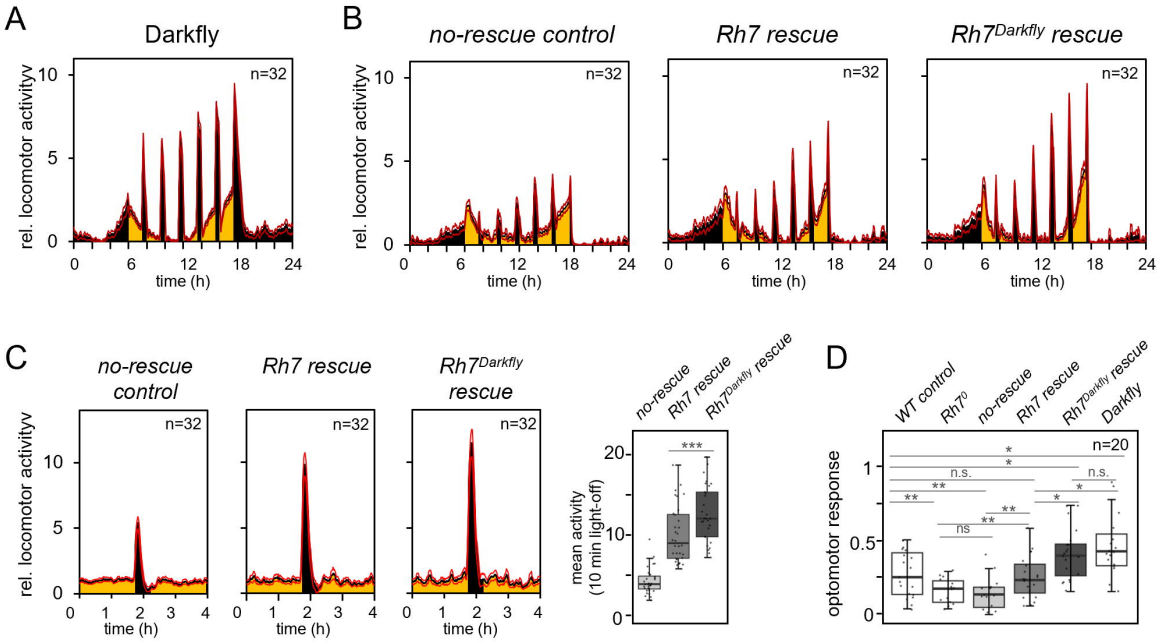
A
Darkfly
rel. locomotor activityv
n=32
time (h)
B
no-rescue control
Rh7 rescue
Rh7Darkfly rescue
C
no-rescue control
Rh7 rescue
Rh7Darkfly rescue
mean activity (10 min light-off)
***
D
WT control
Rh70
no-rescue
Rh7 rescue
Rh7Darkfly rescue
Darkfly
optomotor response
n=20
n.s.
ns

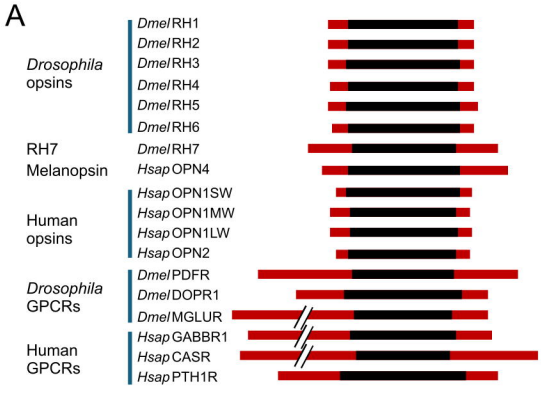
A
Drosophila opsins
Dmel RH1
Dmel RH2
Dmel RH3
Dmel RH4
Dmel RH5
Dmel RH6
RH7
Dmel RH7
Melanopsin
Hsap OPN4
Human opsins
Hsap OPN1SW
Hsap OPN1MW
Hsap OPN1LW
Hsap OPN2
Drosophila GPCRs
Dmel PDFR
Dmel DOPR1
Dmel MGLUR
Human GPCRs
Hsap GABBR1
Hsap CASR
Hsap PTH1R

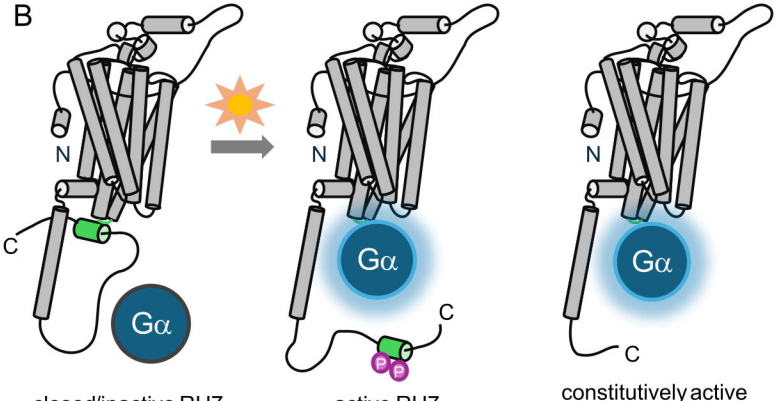
B
N
C
Gα
P
P
closed/inactive RH7
active RH7
constitutively active RH7 in Darkfly